To the Graduate Council:
I am submitting herewith a dissertation written by Cem Özen entitled "Shell Model Monte Carlo Method in the $pn-$formalism". I have examined the final paper copy of this dissertation for form and content and recommend that it be accepted in partial fulfillment of the requirements for the degree of Doctor of Philosophy, with a major in Physics.

Witek Nazarewicz, Major Professor

We have read this dissertation
and recommend its acceptance:

Accepted for the Council:

Vice Chancellor and Dean of
Graduate Studies

Thesis
2005b
.094

Shell Model Monte Carlo Method in the $pn-$formalism

A Dissertation
Presented for the
Doctor of Philosophy
Degree
The University of Tennessee, Knoxville

Cem Özen
August 2005

Dedication

This dissertation is dedicated to my mother Gökçen Özen, and to my grandfather Vehbi Fehmi Sürat.

Acknowledgments

First and foremost, I would like to thank my family, in particular, my mother Gökçen deeply from my heart for having encouraged me to become a scientist since my childhood and having always stood by me.

I would like to thank my advisor David Dean who introduced me to various computational methods of the many-body physics, and inspired my interest in interdisciplinary applications. I express my gratitude to Witek Nazarewicz for many insightful discussions I had the chance to have during my doctoral studies. I also owe thanks to the other members of the Nuclear Theory Group of the ORNL Physics Division, in particular, Thomas Papenbrock and Mario Stoitsov and postdocs Gergana Stoitcheva, Andrius Juodagalvis and Karim Bennaceur. I am also grateful to Carrol Bingham and Bob Compton for their useful comments on my dissertation.

I would like to express my appreciation of Althea Tate who proofread the manuscript, and Judy Hutchins and Pam Carter who were always helpful on administrative issues.

Through the years I spent in Knoxville, I had many great friends who made this city a second home for me. Although it is impossible to name all of them here, I cannot help but thank Marco Congedo ("Pasha"), Hussein and Kunka, Chad and Serpil, "little" Yussef and "big" Yussef, Chris, Renee and Laurent, Fosca, Ryoko, Indraneel, Ulla, Megan, Matt, Marty, Anibal, Lourdes, Tasha, Stoyan, Brandon, and of course my dear brother Can and his wife Aysu for making life always colorful and enjoyable.

Last but not least, I am deeply indebted to my girlfriend Dilek Koyuncu for her patience. Her presence in my life inspired the strength and encouragement at those times when I needed them the most.

Abstract

We report on the development of a new shell-model Monte Carlo algorithm, which uses the proton-neutron formalism. Shell model Monte Carlo methods, within the isospin formulation, have been successfully used in large-scale shell-model calculations. Motivation for this work is to extend the feasibility of these methods to shell-model studies involving non-identical proton and neutron valence spaces. We show the viability of the new approach with some test results. Finally, we use a realistic effective nucleon-nucleon interaction in the model space described by $(1p_{1/2}, 0g_{9/2})$ proton and $(1d_{5/2}, 2s_{1/2}, 1d_{3/2}, 0g_{7/2}, 0h_{11/2})$ neutron orbitals above the ^{88}Sr core to calculate ground-state energies, binding energies, $B(E2)$ strengths, and study pairing properties of the even-even $^{90-104}$Zr and $^{92-106}$Mo isotope chains.

Contents

1 Introduction 1

2 Overview of Nuclear Shell Model 4

3 Monte Carlo Methods 10
- 3.1 The Hubbard-Stratonovich Transformation . . . 10
- 3.2 Quadratization of the Hamiltonian . . . 14
  - 3.2.1 Isospin formalism vs. proton-neutron formalism . . . 18
- 3.3 Monte Carlo Methods . . . 19
- 3.4 Calculation of Static Observables . . . 25
  - 3.4.1 Projecting onto good A and T_z states . . . 26
  - 3.4.2 Projecting onto good parity states . . . 30
- 3.5 The Monte Carlo Sign Problem . . . 31
  - 3.5.1 A practical solution to the sign problem . . . 35

4 Numerical Results 38
- 4.1 Test Cases . . . 38
- 4.2 Applications on Zr and Mo Isotope Chains . . . 42
  - 4.2.1 Ground-state energies . . . 42
  - 4.2.2 Binding energies . . . 45
  - 4.2.3 $B(E2)$ strengths . . . 47
  - 4.2.4 Pairing properties . . . 47

5 Summary and Conclusions 52

Bibliography 54

Vita 59

List of Tables

2.1 Shell-model dimensions for typical nuclei for various major shells. Dimensions are given for $M = 0$ states [4]. 8

4.1 Comparison of the ground-state energies (in MeV), as calculated by SMMCpn and the ANTOINE results. A quadrupole interaction is used. 39

4.2 Comparison of the ground-state energies (in MeV), as calculated by SMMCpn and the ANTOINE results. A quadrupole plus pairing interaction is used. 40

4.3 Comparison of exact diagonalization, SMMCpn, and isospin SMMC results for ground-state energies (in MeV) and $B(E2)$ strengths (in e^2fm^4). Typical error bar for energies is ± 0.6 MeV for SMMCpn and ± 0.4 MeV for isospin SMMC calculations. 41

4.4 Comparison of exact diagonalization, SMMCpn, and isospin SMMC results for $B(M1)$ (in μ_N) and Gamow-Teller strengths. 41

4.5 Physical parameters used in the calculations 43

List of Figures

2.1 Emergence of shell structure 5
2.2 Evolution of CPU speed of computers and shell-model dimension [4]. 9

3.1 Extrapolation of some observables for ^{48}Ti 37

4.1 Ground-state energies of the even-even $^{90-104}$Zr and $^{92-106}$Mo isotopes. Results from direct diagonalization available for lighter isotopes are also shown. 44
4.2 Binding energies of the even-even $^{90-104}$Zr and $^{92-106}$Mo isotopes . . . 46
4.3 Total $B(E2)$ strengths (from the ground state) of the even-even $^{90-104}$Zr and $^{92-106}$Mo isotopes. Experimental results are for $0_1^+ \dashrightarrow 2_1^+$ 48
4.4 Pairing correlations of the even-even $^{90-104}$Zr and $^{92-106}$Mo isotopes. Fermi-gas values are subtracted. 49
4.5 Orbital occupation numbers of the even-even $^{90-104}$Zr and $^{92-106}$Mo isotopes 51

Chapter 1

Introduction

The physics of nuclei covers a vast arena of diverse phenomena and proved to be extremely challenging through its history from its early days of the discovery of neutron till today. A large number of models have been developed to address different classes of problems. Among these models, the nuclear shell model has a very central role capable of addressing all aspects of the nuclear many-body problem.

One of the computational techniques developed for the nuclear shell model, the shell model Monte Carlo (SMMC) method [36, 37] is a powerful tool that has been succesfully used in large-scale applications. The subject matter of this thesis is to to report on the development of a new SMMC algorithm, based on the $pn-$formalism, in order to extend the applicability of the method to shell model calculations where the isospin symmetry is not manifest in the effective NN interactions.

The early form of the nuclear shell model was introduced in 1949 [6, 43] as an independent particle model and succesfully explained nuclear regularities associated with the existence of magic numbers, and other properties such as spins and magnetic moments of nuclei in the vicinity of magic shell closures. However as the neutron or proton numbers depart from the magic numbers, the independent particle picture fails to be satisfactory, and configuration mixing arising from the interactions among the valence orbitals becomes essential. Thus the interacting shell model was formulated to produce such mixing of many-body configurations and the shell model has been a subdiscipline of the many-body problem. During the past few decades, our knowledge of in-medium nucleon-nucleon interaction has increased noticeably and thanks to advances in computer speeds and memory, the shell model has been applied succesfully to many nuclei close to and far from the valley of stability. It has thus proved to be capable of explaining a wide range of phenomena related to both single-particle and collective degrees of freedom [4, 8, 11], hence providing a unified view of nuclear structure physics. The conventional method of solution for the shell model is the diagonalization of the Hamiltonian matrix constructed for many-body basis vectors.

This can be done either in uncoupled angular momentum (m-scheme) or coupled scheme (J-scheme), and a number of computer codes have been developed based on either approaches. However, combinatorial scaling of the many-body space with the single-particle basis and number of valence nucleons limits such an approach to light nuclei, or to heavier nuclei with a small number of valence nucleons. In recent decades, alternative approaches such as stochastic methods for the path integral formulation, density matrix renormalization group (DMRG) [23, 54] and the coupled cluster method [15, 20, 38, 66], have been proposed to overcome these computational limitations in large-scale computations. Stochastic approaches include the quantum Monte Carlo (QMC) method [55, 56] for the *ab initio* calculations of light nuclei, and the SMMC, and the Monte Carlo shell model (MCSM) [51, 52] methods for calculations involving large valence spaces.

The SMMC method is based on the idea of representing the partition function of the nuclear system as a path integral of the coherent superposition of one-body evolution operators in fluctuating one-body fields. This is achieved by applying the Hubbard-Stratonovich transformation [33] to the imaginary-time many-body evolution operator. The resulting integral is then evaluated stochastically using the Metropolis algorithm [44]. This approach can deal with much larger valence spaces than conventional approaches. Since it calculates ensemble averages, the SMMC method is not a suitable tool to provide detailed spectroscopy, with the exception of the ground state expectation values which can be calculated in the low temperature limit. However, it can calculate many nuclear properties such as masses, total strengths, strength distributions, and deformation. One apparent limitation of the SMMC approach is the "sign problem" causing non-positive definite integrands leading to intractable statistical errors. However, this problem can be either be circumvented via an extrapolation method [2] or delayed via the shifted-contour method [59]. There is even a well known class of schematical interactions free of the sign problem, which contains most relevant content of the realistic interactions for the calculation of certain properties of nuclei, such as level densities.

In recent years, we have witnessed an increased interest in nuclei far from the valley of stability. New experimental facilities are pushing the boundaries of known nuclei towards the proton and neutron drip-lines . In such heavy regimes where the shell model calculations are often not feasible, mean-field methods are the main theoretical tools providing the bulk properties of the nuclei. However shell model predictions for those regions can be tested in heavy nuclei that lie closer to the line of stability, where such calculations are possible through SMMC methods. It is also important to test realistic effective interactions adopted to valence spaces designed for some regions of heavy nuclei. SMMC methods are also very helpful in astrophysical applications such as nuclear beta-decay and electron capture rate calculations. Such applications often involve conditions of extreme temperatures and densities, and are generally

beyond the reach of experimental capabilities. Since exact diagonalization methods are not applicable due to enermous size of the valence spaces, SMMC have often been the most available, if not the only, means of calculation which is a natural one also because SMMC methods are designed to calculate thermal expectation values.

For heavy nuclei, or nuclei far from the valley of stability, shell-model calculations often involve proton and neutron valence spaces that may have only a few or no common orbitals; hence, despite the underlying NN-interaction is isospin invariant, the effective interaction in the valence space does not respect this symmetry, in which case the current isospin SMMC code is no longer applicable to calculations of such systems. In this work, we first outline the SMMC method in the $pn-$formalism and then demonstrate its computational power in an application to even-even $^{90-104}$Zr and $^{92-106}$Mo isotope chains. In this mass region, occupancies of the single-particle configurations are known to be related to sudden changes in nuclear properties such as quadrupole deformation as a function of neutron and proton numbers and a study of these isotopes may give new insights about the evolution of the shell structure and a test ground for the shell model interactions in this mass region.

Chapter 2

Overview of Nuclear Shell Model

In this chapter we will give a brief introduction to the nuclear shell model starting from the basic notion of a mean field and shell structure, and then we will outline important tenets of a typical shell-model calculation. Then the current status of the conventional shell-model calculations will be summarized. A detailed treatment of the nuclear shell-model problem can be found in any one of the books in references [10,30,41,60].

Essential to the nuclear shell model is the idea of a central potential. The early form of the shell model was able to explain the shell structure and the bulk properties of the nuclei in the immediate vicinity of magic closures, according to a picture in which nucleons are independent particles confined by a central harmonic oscillator potential with a strong spin-orbit coupling:

$$U(r) = \frac{1}{2}\hbar\omega r^2 + D\vec{l}^2 + C\vec{l}\cdot\vec{s}. \tag{2.1}$$

This potential generates single particle levels which then are filled, starting from the lowest one up to the shell gap. Then the wave function of the ground state is expressed as the product of the two Slater determinants, one for the neutrons and another for the protons. As we add more protons and neutrons thereby departing from the magic numbers, this picture becomes too simple to explain nuclear properties and it becomes clear that "residual interaction" between nucleons is essential to mix different configurations and thus break the degeneracies inherent to the filling of the orbitals by two or more nucleons.

In this interacting shell model, the nuclear Hamiltonian for a nucleus made of A nucleons can be written as

$$\begin{aligned}\hat{H} &= \sum_i \hat{t}_i + \frac{1}{2}\sum_{ij}\hat{v}_{ij} = \sum_i(\hat{t}_i + \hat{U}_i) + \frac{1}{2}\sum_{ij}(\hat{v}_{ij} - 2\hat{U}_i\delta_{ij}) \\ &= \hat{H}_0 + \hat{H}_{res}. \end{aligned} \tag{2.2}$$

Above, we have introduced the concept of "residual interaction" in connection with the mean-field (*i.e.* central) potential. The mean-field potential can be chosen to be a harmonic oscillator, Woods-Saxon, or Hartree-Fock potential. The nucleons are assumed to be interacting via a two-body NN interaction, which can be generated from a microscopic level and at this stage will be taken as a basic ingredient of our model. Fig. 2.1 illustrates the single-particle orbitals produced by the potential U_i. A striking observation about the distribution of the orbitals is the grouping of levels (*i.e.* shells) and the existence of well-defined gaps between them. The orbitals are labeled through the quantum numbers $\{nljt_z\}$, where n denotes the principal quantum number, l the orbital angular momentum, j the total angular momentum, and t_z the $z-$component of the isospin of the nucleon. Each orbital has a degeneracy of $2j+1$. Hence, single-particle levels in an orbital have an additional m quantum number for the $z-$component of the total angular momentum. The single-particle levels in a given shell have, in general, the same parity and same major oscillator quantum number. As already mentioned in the Introduction, shell-model calculations are restricted by computational limitations which make certain approximations unavoidable. Firstly, due to large shell gaps, we generally impose restrictions on the number of nucleons that can be excited, and secondly, we may truncate the infinite

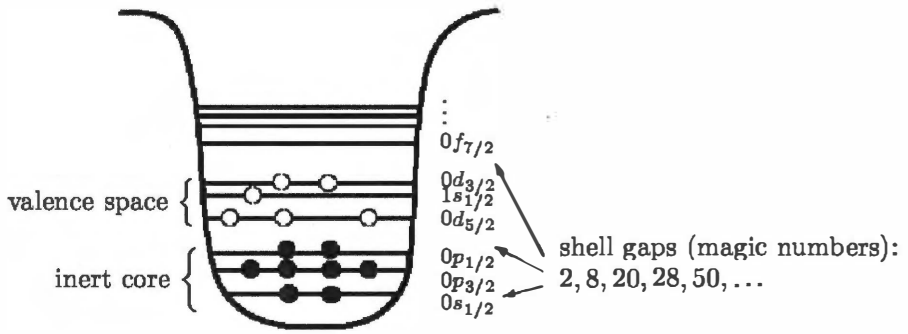


Figure 2.1: Emergence of shell structure

Hilbert space to render the problem tractable. The concept of an inert *core* emerges by filling the single-particle levels from the $0s_{1/2}$ orbital up to a certain orbit right below a shell gap at a magic number. Nucleons occupying the core will be "frozen", *i.e.* they will not be excitable to orbitals above the shell gap. Since the core is comprised of completely occupied single-particle levels, it is isotropic and has the spin-parity $J^\pi = 0^+$, like a vacuum, and apart from its contribution in the spherical mean field and the renormalization of operators, the nucleons occupying the core do not play an explicit role in the shell model calculations. (For light nuclei ($A \sim 12$), shell-model calculations can cope with the dimensions of the model space without the need to have an inert core; hence, they are called the no-core shell-model calculations [24, 46].) The nucleons outside the core are called the *valence* nucleons. Due to the same computational limitations, the valence nucleons will be allowed to occupy only a few single-particle orbitals above the core, typically one major oscillator shell, which defines the valence space. The concepts of the core and valence space are theoretical idealizations, but their utilization is supported by the fact that the most significant components of the low-lying states of nuclei can be thought of as many-body configurations containing excitations of the nucleons into a few orbitals in the neighborhood of the Fermi level.

Now we can specify a shell model procedure: Choose a proper valence space, adopt an effective interaction to it, and solve the eigenvalue problem with an efficient algorithm [9, 11, 21, 31].

Conventionally, model spaces are defined in terms of the shell gaps associated with the LS oscillator scheme, which are observed experimentally at 2, 8, 20, 28, 50, 82, 126 ... defining the $0s$, $0p$, $1s$-$0d$, $1p$-$0f$ ... shells. However, choosing a suitable model space may not be obvious in the case of heavy nuclei, in particular, nuclei that are far from the β-stability line, for which shell gaps may be reduced, modified, or even disappear. Particularly, for heavy nuclei, the LS oscillator scheme is broken by the spin-orbit interaction, which is responsible for the exchange of the orbitals of highest j in two subsequent oscillator shells. In certain mass regions, the break-up of the oscillator scheme poses a challenge for future applications. Also, far from the β-stability line, the single-particle levels may have considerably changing energy spacings with the increasing number of protons or neutrons. This may result in the replacement of the well-known magic numbers 8, 20, 28 ... with 6, 16, 34 ... in neutron-rich nuclei [53].

In a suitably chosen valence space, one can obtain a regularized effective interaction through the G-matrix approach, starting from the bare NN-force. However, the G-matrix method often requires some phenomenological corrections, particularly for the single-particle energies, and also it is known to work better in no-core calculations, and for model spaces with a small number of valence particles. Truncation of

the infinite Hilbert space into the valence space necessarily implies the introduction of effective operators through a renormalization procedure:

$$\hat{H}|\Psi\rangle = E|\Psi\rangle \rightarrow \hat{H}_{eff}|\Psi_{eff}\rangle = E|\Psi_{eff}\rangle. \tag{2.3}$$

Once a good valence space and an effective interaction suitable for it have been determined, one aims to solve the secular equation to obtain as much physical information as possibly available by the method of solution. Therefore, as long as computationally feasible, the method of solution should be the exact diagonalization of Eqn. 2.3. For this purpose, the Lanczos algorithm has become a standard, as it is very efficient for the computation of the low-lying eigenvectors, which are the most important for nuclear structure calculations.

Existing computer codes performing exact diagonalization fall into two main categories:

- m-scheme:
  Glasgow-Manchester code [65], ANTOINE [13], OXBASH [57] *etc.*
- the coupled scheme (J or JT):
  Oak-Ridge/Rochester code [25], Drexel University code (DUSM) [14],
  NATHAN [48] *etc.*

The m-scheme approach uses the Slater determinants of A particles distributed in k individual single-particle states as its basis states. Since fermionic occupation numbers for an individual single particle state can only take the values 0 or 1, each Slater determinant can be represented naturally in the form of an integer word, of which every bit is associated with a single particle state. Despite its simplicity, the m-scheme approach has the disadvantage that J and T are not good quantum numbers; hence, the dimensions of the matrices are maximal, i.e., the space contains all states with $J \geq J_z$ and $T \geq T_z$. For large model spaces, a coupling scheme (J or JT) is, in general, more efficient in terms of memory because the full m-scheme matrix is reduced to boxes of smaller dimensions of good J (or JT) quantum number. In general, this reduces the memory requirements considerably but the price to pay is the necessity of computing the coefficients of fractional parentage. Considering the overall efficiency, however, the two approaches are complementary to each other depending on the nature of the shell-model calculation. Typically coupled codes are used for low J calculations.

Feasibility of the traditional diagonalization methods, whether based on the m-scheme or the coupled scheme, is limited by the number of many-body basis states which can grow very quickly with the number of valence particles or the dimension of the valence space. One can see this by calculating the total number of Slater

Table 2.1: Shell-model dimensions for typical nuclei for various major shells. Dimensions are given for $M = 0$ states [4].

shell	# of single-particle states	nucleus	$M = 0$ states
p	6	^{10}B	84
sd	12	^{28}Si	9.4×10^4
fp	20	^{60}Zn	2.0×10^9
$50 \leq Z, N \leq 82$	32	^{132}Dy	$\sim 10^{16}$
$50 \leq Z \leq 82, 82 \leq N \leq 126$	32,44	^{170}Dy	$\sim 10^{20}$

determinants within a Hilbert space, which can give a rough estimate of the dimension of the m-scheme or coupled scheme spaces

$$D = \begin{pmatrix} N_{s\pi} \\ \pi \end{pmatrix} \begin{pmatrix} N_{s\nu} \\ \nu \end{pmatrix}. \tag{2.4}$$

Above $N_{s\pi}$ and $N_{s\nu}$ are the number of single-particle states for protons and neutrons, and π and ν are the number of valence protons and neutrons, respectively. The actual dimension of the m-scheme, D_m, or of the coupled scheme, D_J, is, in fact, several orders of magnitude smaller than the number D given by Eqn. 2.4, as the z-component of the angular momentum is fixed in the m-scheme and we project states of good angular momentum in the J-scheme. Take the example of the mid-fp shell nucleus ^{60}Zn. Eqn. 2.4 gives $D \approx 3.4 \times 10^{10}$ Slater determinants. The dimension of $M = 0$ states is approximately 2.0×10^9, whereas the dimension of $J = 0$ states is of the order of 10^7 [49]. In Table 2.1, the m-scheme dimensions for $M = 0$ states for some major shells are shown.

As seen in Table 2.1, the enormous increase in shell-model dimensions suggests that regardless of possible advances in computational power in the future, shell-model calculations for many nuclei will lie well beyond the reach of feasibility. Fig. 2.2 shows the increase in the floating point computational speed in Gflops through years. A number of shell-model applications and the corresponding m-scheme dimensions are also indicated. One can see that, roughly speaking, the computational power has doubled every two years. Nowadays, ANTOINE and NATHAN codes can deal with matrix dimensions $D_m \sim 10^9$ and $D_J \sim 10^7$, respectively.

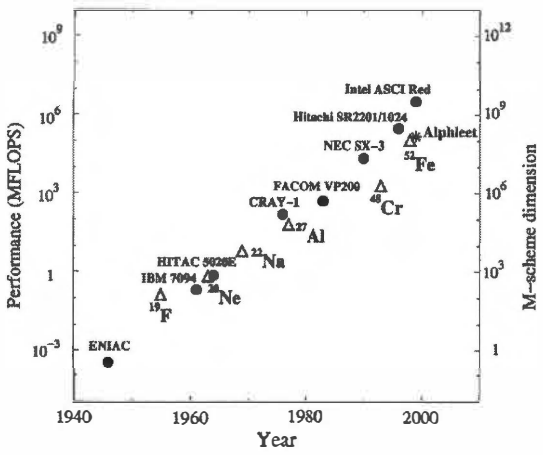


Figure 2.2: Evolution of CPU speed of computers and shell-model dimension [4].

In contrast to the conventional diagonalization methods, the numerical effort required by the SMMC method scales much more gently with the dimension of the valence space, and it is independent of the number of valence nucleons. Moreover, it is parallelizable in a straightforward fashion. Thus, SMMC renders much larger shell-model calculations amenable than the largest calculations that can be done using the conventional diagonalization. In this chapter we have summarized the basics of a nuclear shell-model calculation and mentioned various traditional methods; now it is time to present the formal description of the SMMC approach which will follow in the next chapter.

Chapter 3

Monte Carlo Methods

3.1 The Hubbard-Stratonovich Transformation

SMMC calculations employ the imaginary-time many-body evolution operator $\hat{U} = e^{-\beta\hat{H}}$ to project out the ground-state properties and evaluate thermal expectation values $\langle\hat{O}\rangle = \mathrm{Tr}(\hat{U}\hat{O})/\mathrm{Tr}\hat{U}$. Above $\beta = 1/kT$ is the inverse temperature. Central to the development of the SMMC technique is the Hubbard-Stratonovich (HS) transformation [33] by which the imaginary-time evolution operator $\hat{U}$ is managed. Here we restrict ourselves to Hamiltonians that have at most two-body terms which can always be cast into the "normal" form as

$$\hat{H} = \sum_i \epsilon_i a_i^\dagger a_i + \frac{1}{2}\sum_\alpha \lambda_\alpha \hat{\rho}_\alpha^2. \tag{3.1}$$

Above ϵ_i is the energy of single-particle level i. The operator $\hat{\rho}_\alpha$ is a linear combination of one-body density operators $\hat{\rho}_{ij} = a_i^\dagger a_j$. Note that the number of operators $\hat{\rho}_\alpha$ can at most be N_s^2, where N_s^2 is the size of the valence space. λ_α are eigenvalues associated with the interaction matrix and they are real. To see what the HS transformation does, we will start with the well-known Gaussian integral identity,

$$e^{-\frac{1}{2}\Delta\beta\lambda\hat{O}^2} = \sqrt{\frac{\Delta\beta|\lambda|}{2\pi}}\int \mathrm{d}\sigma\; e^{-\frac{1}{2}\Delta\beta|\lambda|\sigma^2 + \Delta\beta s\sigma\lambda\hat{O}}, \tag{3.2}$$

where $s = \pm 1$ if $\lambda > 0$, or $s = \pm i$ if $\lambda < 0$. This identity shows how the evolution operator $\hat{U}$ can be linearized by introducing an auxiliary field σ_α for each operator $\hat{O}_\alpha$:

$$e^{-\beta\hat{H}} \approx \int \prod_{\alpha} \sqrt{\frac{\beta|\lambda_\alpha|}{2\pi}}\, \mathrm{d}\sigma_\alpha(\tau)\; e^{-\frac{1}{2}\beta\sum_\alpha |\lambda_\alpha|\sigma_\alpha^2} e^{-\beta\hat{h}(\sigma)}, \tag{3.3}$$

where

$$\hat{h}(\sigma) = \sum_i \epsilon_\alpha a_i^\dagger a_i + \sum_\alpha s_\alpha \lambda_\alpha \sigma_\alpha \hat{\rho}_\alpha. \tag{3.4}$$

However, since, in general, $[\hat{O}_\alpha, \hat{O}_\beta] \neq 0$, direct use of the identity in Eqn. 3.3 would be inappropriate. Therefore we split the time interval $[0, \beta]$ into N_t time slices and write the operator $\hat{U}$ as

$$e^{-\beta\hat{H}} = (e^{-\Delta\beta\hat{H}})^{N_t}. \tag{3.5}$$

Now we can use the identity since the error terms due to the non-vanishing commutators are of order $(\Delta\beta)^2$. We label time slices such that $\tau_n = n\Delta\beta$ for $n = 1 \ldots N_t$, and introduce a different set of auxiliary field $\sigma_\alpha(\tau_n)$ for each time slice to obtain the HS representation of the operator $\hat{U}$:

$$e^{-\beta\hat{H}} = \int \mathcal{D}[\sigma] G_\sigma \hat{U}_\sigma, \tag{3.6}$$

where the metric of the functional integral is given by

$$\mathcal{D}[\sigma] = \prod_{\alpha,n} \sqrt{\frac{\Delta\beta|V_\alpha|}{2\pi}} \mathrm{d}\sigma_\alpha(\tau_n), \tag{3.7}$$

and the Gaussian weight above is defined as

$$G_\sigma = e^{-\frac{1}{2}\Delta\beta\sum_{\alpha,n}|v_\alpha|\sigma_\alpha^2(\tau_n)}. \tag{3.8}$$

Note that the resulting path integral representation in the auxiliary fields σ has a one-body evolution operator

$$\hat{U}_\sigma = e^{-\Delta\beta\hat{h}_\sigma(\tau_{N_t})} \cdots e^{-\Delta\beta\hat{h}_\sigma(\tau_1)} \equiv \mathcal{T} e^{-\int_0^\beta d\tau \hat{h}_\sigma(\tau)}, \tag{3.9}$$

where the linearized Hamiltonian is defined by

$$\hat{h}_\sigma(\tau_n) = \sum_i \epsilon_\alpha a_i^\dagger a_i + \sum_\alpha s_\alpha \lambda_\alpha \sigma_\alpha(\tau_n) \hat{\rho}_\alpha. \tag{3.10}$$

Now the thermal expectation value of an operator $\hat{O}$ can be expressed in the HS representation as

$$\langle \hat{O} \rangle = \frac{\mathrm{Tr}[\hat{O}e^{-\beta\hat{H}}]}{\mathrm{Tr}[e^{-\beta\hat{H}}]} = \frac{\int \mathcal{D}[\sigma] G_\sigma \langle \hat{O} \rangle_\sigma \xi_\sigma}{\int \mathcal{D}[\sigma] G_\sigma \xi_\sigma}, \tag{3.11}$$

where the following definitions are used:

$$\xi_\sigma = \mathrm{Tr}\hat{U}_\sigma; \qquad \langle \hat{O} \rangle_\sigma = \frac{\mathrm{Tr}[\hat{O}\hat{U}_\sigma]}{\mathrm{Tr}\hat{U}_\sigma}. \tag{3.12}$$

According to the definition above, $\langle \hat{O} \rangle_\sigma$ can be interpreted as the expectation value of the operator $\hat{O}$ in a non-interacting system of fermions moving in fluctuating mean fields $\sigma(\tau)$. This is the crucial outcome of the HS representation, by which the two-body interactions in the Hamiltonian are linearized with the introduction of fluctuating auxiliary fields. The resulting one-body traces, as we shall see later on, can be evaluated by manipulations of matrices of dimension $N_s \times N_s$ where N_s is the size of the valence space, including both proton and neutron single-particle levels. This is how the many-body problem is rendered "tractable". At each time slice, we have introduced an auxiliary field for each λ_α whose number can be at most N_s^2. Thus the dimension of the multi-dimensional integrals in fluctuating fields is of the order of $N_s^2 N_t$. These integrals can be evaluated using Monte Carlo methods, the basics of which will be summarized in Sec. 3.3. In particular, the Metropolis algorithm will be described as a suitable way of generating the auxiliary fields to perform the integrations stochastically.

In order to use Monte Carlo methods, we need to define a positive-definite weight function

$$W_\sigma = G_\sigma |\xi_\sigma|, \tag{3.13}$$

so now Eqn. 3.11 can be rewritten as

$$\langle \hat{O} \rangle = \frac{\int \mathcal{D}[\sigma] W_\sigma \langle \hat{O} \rangle_\sigma \Phi_\sigma}{\int \mathcal{D}[\sigma] W_\sigma \Phi_\sigma} \equiv \frac{\langle \langle \hat{O} \rangle_\sigma \Phi_\sigma \rangle_W}{\langle \Phi_\sigma \rangle_W}, \tag{3.14}$$

where

$$\Phi_\sigma = \frac{\xi_\sigma}{|\xi_\sigma|} \tag{3.15}$$

is the sign of the partition function.

Note that we have expressed the integrals in Eqn. 3.14 as W-weighted averages. Performing a random walk in the $\vec{\sigma}$ space, we can generate a statistically independent set of auxiliary fields $\{\sigma_k : k = 1, \ldots, N\}$ distributed according to the weight function W_σ, and thus write the W-weighted average of any σ-dependent function X as

$$\langle X_\sigma \rangle = \frac{\int \mathcal{D}[\sigma] W_\sigma X_\sigma}{\int \mathcal{D}[\sigma] W_\sigma} \approx \frac{1}{N} \sum_k^N X_{\sigma_k}. \tag{3.16}$$

Thus, we can write the Monte Carlo result for the observable O in Eqn. 3.14 as

$$\langle \hat{O} \rangle_{\mathrm{MC}} \approx \frac{\sum_k \langle \hat{O} \rangle_{\sigma_k} \Phi_{\sigma_k}}{\sum_k \Phi_{\sigma_k}}, \tag{3.17}$$

up to a statistical error given by

$$\delta \langle \hat{O} \rangle_{\mathrm{MC}} = \frac{1}{\sqrt{N}} \left[\frac{\langle \hat{O}^2 \Phi^2 \rangle - \langle \hat{O} \Phi \rangle^2}{\langle \Phi \rangle^2} + \frac{\langle \hat{O} \Phi \rangle^2}{\langle \Phi \rangle^4} (\langle \Phi^2 \rangle - \langle \Phi \rangle^2) \right.$$
$$\left. -2 \frac{\langle \hat{O} \Phi \rangle}{\langle \Phi \rangle^3} (\langle \hat{O} \Phi^2 \rangle - \langle \Phi \rangle \langle \hat{O} \Phi \rangle) \right]^{1/2}. \tag{3.18}$$

The uncertainity above is estimated from the variance of the "observations" $\langle \hat{O} \rangle_{\sigma_k}$. We have taken into account the correlations of $\langle \hat{O} \rangle_{\sigma_k}$ with Φ_{σ_k} since both are calculated from the same set of fields.

3.2 Quadratization of the Hamiltonian

We have seen in the section above that, to utilize the HS representation, we need to cast the two-body part of the Hamiltonian into a quadratic form using an appropriate set of operators. The set of operators can be chosen as linear combinations of one-body density operators or linear combinations of pair creation and annihilation operators. The first approach is called the density decomposition, and the latter the pairing decomposition. We can exemplify both ways of decomposition on an individual interaction term [39]:

$$\hat{H} = a_1^\dagger a_2^\dagger a_3 a_4. \tag{3.19}$$

Let's start with the density decomposition. There are two possible ways of doing this, either by grouping (1,3) and (2,4) to obtain

$$\begin{aligned} \hat{H} &= \overbrace{a_1^\dagger a_3}\, \underbrace{a_2^\dagger a_4} - a_1^\dagger a_4 \delta_{23} \\ &= -a_1^\dagger a_4 \delta_{23} + \frac{1}{2}[a_1^\dagger a_3, a_2^\dagger a_4] + \frac{1}{4}(a_1^\dagger a_3 + a_2^\dagger a_4)^2 \\ &\quad -\frac{1}{4}(a_1^\dagger a_3 - a_2^\dagger a_4)^2, \end{aligned} \tag{3.20}$$

or grouping (1,4) and (2,3) to obtain

$$\hat{H} = -\overbrace{a_1^\dagger a_4}\, \underbrace{a_2^\dagger a_3} + a_1^\dagger a_3 \delta_{24} \tag{3.21}$$

$$\begin{aligned} &= a_1^\dagger a_3 \delta_{24} - \frac{1}{2}[a_1^\dagger a_4, a_2^\dagger a_3] - \frac{1}{4}(a_1^\dagger a_4 + a_2^\dagger a_3)^2 \\ &\quad + \frac{1}{4}(a_1^\dagger a_4 - a_2^\dagger a_3)^2. \end{aligned} \tag{3.22}$$

Alternatively in the pairing decomposition, one groups pair creation and annihilation operators together:

$$\hat{H} = \overbrace{a_1^\dagger a_2^\dagger} \underbrace{a_4 a_3} \tag{3.23}$$

$$= \frac{1}{4}(a_1^\dagger a_2^\dagger + a_3 a_4)^2 - \frac{1}{4}(a_1^\dagger a_2^\dagger - a_3 a_4)^2 + \frac{1}{2}[a_1^\dagger a_2^\dagger, a_3 a_4]. \tag{3.24}$$

All the commutator terms above are one-body operators, and they should be added to the one-body term of the Hamiltonian. This example has thus shown that it is possible to transform the two-body part of a general Hamiltonian into a quadratic form. Although we mention the pairing decomposition for purposes of completeness, we will follow the density decomposition approach. But in principle, it is possible to use either approach, or both at the same time, since the resulting path-integral is independent of the way the Hamiltonian is decomposed.

In the following, we have adopted a notation that α labels a single-particle level with the quantum numbers $nljm\tau$, where τ signifies either a proton ($\tau = \pi, t_z = -1/2$) or a neutron ($\tau = \nu, t_z = 1/2$). a labels an orbital with the quantum numbers $nlj\tau$. Let us start applying the density decomposition to a general shell-model Hamiltonian $\hat{H} = \hat{H}_1 + \hat{H}_2$, where

$$\hat{H}_1 = \sum_\alpha \epsilon_\alpha a_\alpha^\dagger a_\alpha \tag{3.25}$$

$$\hat{H}_2 = \frac{1}{2}\sum_{\alpha\beta\gamma\delta} V_{\alpha\beta\gamma\delta} a_\alpha^\dagger a_\beta^\dagger a_\delta a_\gamma. \tag{3.26}$$

The nucleon-nucleon interaction must obey rotational and time-reversal invariance, and respect parity conservation. It is convenient to write the Hamiltonian in such a way that the rotational invariance and shell structure are explicit:

$$\hat{H}_2 = \frac{1}{4}\sum_{abcd}\sum_J [(1+\delta_{ab})(1+\delta_{cd})]^{1/2} V_J^A(ab,cd) \times \sum_M \hat{A}_{JM}^\dagger(ab)\hat{A}_{JM}(cd), \tag{3.27}$$

where $V_J^A(ab,cd)$ are the anti-symmetrized two-body interaction matrix elements in the J-coupled scheme satisfying:

$$V_J^A(ab,cd) = -(-1)^{j_a+j_b-J} V_J^A(ba,cd) = -(-1)^{j_c+j_d-J} V_J^A(ab,dc). \tag{3.28}$$

The pair creation and annihilition operators in this J-coupled scheme are defined as

$$\begin{aligned} \hat{A}^\dagger_{JM}(ab) &= \sum_{m_a m_b} (j_a m_a j_b m_b | JM) a^\dagger_{j_b m_b \tau_b} a^\dagger_{j_a m_a \tau_a} \\ &= -[a^\dagger_{j_a \tau_a} \otimes a^\dagger_{j_b \tau_b}]^{J,M}, \qquad (3.29) \\ \hat{A}_{JM}(ab) &= \sum_{m_a m_b} (j_a m_a j_b m_b | JM) a_{j_a m_a \tau_a} a_{j_b m_b \tau_b} \\ &= [a_{j_a \tau_a} \otimes a_{j_b \tau_b}]^{J,M}. \qquad (3.30) \end{aligned}$$

Note that, in general, isospin invariance can also be made explicit in Eqn. 3.27, as done in [37, 39]. However, as we mentioned earlier, effective interactions derived for non-identical proton and neutron valence spaces break this symmetry. Since it is our aim to deal with such cases, we are not going to follow that approach.

The Hamiltonian in Eqn. 3.27 can be expressed in diagonal quadratic form in terms of density operators with definite multipolarity defined as

$$\hat{\rho}_{KM}(ab) = \sum_{m_a m_b} (j_a m_a j_b m_b | KM) a^\dagger_{j_a m_a \tau_a} \tilde{a}_{j_b m_b \tau_b} = [a^\dagger_{j_a \tau_a} \otimes \tilde{a}_{j_b \tau_b}]^{K,M}, \tag{3.31}$$

where we have used the definition of time-reversed operators,

$$\tilde{a}_{j_a m_a \tau_a} = (-1)^{j_a+m_a} a_{j_a -m_a \tau_a}, \qquad \tilde{a}^\dagger_{j_a m_a \tau_a} = (-1)^{j_a+m_a} a^\dagger_{j_a -m_a \tau_a}. \tag{3.32}$$

Performing a Pandya transformation [10], the two-body part of the Hamiltonian can be decomposed as $\hat{H}_2 = \hat{H}'_2 + \hat{H}'_1$, such that

$$\begin{aligned} \hat{H}'_1 &= \sum_{ad} \epsilon'_{ad} \hat{\rho}_{00}(a,d) \qquad (3.33) \\ \hat{H}'_2 &= \frac{1}{2} \sum_{abcd} \sum_K E_K(ac,bd) \sum_M (-1)^M \hat{\rho}_{KM}(ac) \hat{\rho}_{K-M}(bd), \qquad (3.34) \end{aligned}$$

where ϵ'_{ad} and $E_K(ac,bd)$ are given by

$$\epsilon'_{ad} = -\frac{1}{4}\sum_b\sum_J(-1)^{J+j_a+j_b}(2J+1)\frac{1}{\sqrt{2j_a+1}} \times V_J^N(ab,bd)\sqrt{(1+\delta_{ab})(1+\delta_{cd})}\,, \tag{3.35}$$

$$E_K(ac,bd) = (-1)^{j_b+j_c}\sum_J(-1)^J(2J+1)\begin{Bmatrix} j_a & j_b & J \\ j_d & j_c & K \end{Bmatrix} \times\frac{1}{2}V_J^N(ab,cd)\sqrt{(1+\delta_{ab})(1+\delta_{cd})}\,. \tag{3.36}$$

We can now rewrite H_2' in Eqn. 3.34 as

$$\hat{H}_2' = \frac{1}{2}\sum_{ij}\sum_K E_K(i,j)\sum_M(-1)^M\hat{\rho}_{KM}(i)\hat{\rho}_{K-M}(j), \tag{3.37}$$

where the notation $i=(ac), j=(bd)$ is used. By diagonalizing the E_K matrix

$$E_K(i,j)v_{K\alpha}(j) = \lambda_{K\alpha}v_{K\alpha}(i), \tag{3.38}$$

and defining

$$\hat{\rho}_{KM}(\alpha) = \sum_i\hat{\rho}_{KM}(i)v_{K\alpha}(i), \tag{3.39}$$

we can represent H_2' as

$$\hat{H}_2' = \frac{1}{2}\sum_{K\alpha}\lambda_{K\alpha}\sum_M(-1)^M\hat{\rho}_{KM}(\alpha)\hat{\rho}_{K-M}(\alpha). \tag{3.40}$$

Forming the following linear combinations of $\hat{\rho}_{KM}(\alpha)$

$$\hat{Q}_{KM}(\alpha) \equiv \frac{1}{\sqrt{2(1+\delta_{M0})}}\left(\hat{\rho}_{KM}(\alpha)+(-1)^M\hat{\rho}_{K-M}(\alpha)\right)\,, \tag{3.41}$$

$$\hat{P}_{KM}(\alpha) \equiv -\frac{i}{\sqrt{2(1+\delta_{M0})}}\left(\hat{\rho}_{KM}(\alpha)-(-1)^M\hat{\rho}_{K-M}(\alpha)\right)\,, \tag{3.42}$$

we finally bring H_2' into the desired form:

$$\hat{H}_2' = \frac{1}{2}\sum_{K\alpha}\lambda_{K\alpha}\sum_{M\geq 0}\left(\hat{Q}^2_{KM}(\alpha)+\hat{P}^2_{KM}(\alpha)\right) . \tag{3.43}$$

The HS transformation applied to the diagonal quadratic form of the nuclear Hamiltonian yields the one-body Hamiltonian $\hat{h}_{\sigma\tau}$ of time step τ_n:

$$\begin{aligned}\hat{h}_{\sigma\sigma'}(\tau_n) &= \sum_{\alpha}\epsilon_\alpha a^\dagger_\alpha a_\alpha + \sum_{ad}\epsilon'_{ad}\hat{\rho}_{00}(ad) \\ &\quad + \sum_{K\alpha} s_{K\alpha}\lambda_{K\alpha}\sum_{M\geq 0\, n}(\hat{Q}_{KM}(\alpha)\sigma_{KM\alpha n} + \hat{P}_{KM}(\alpha)\sigma'_{KM\alpha n}).\end{aligned} \tag{3.44}$$

Since we have two quadratic terms in H_2', we need two sets of auxiliary fields, namely $\sigma_{KM\alpha n}$ and $\sigma'_{KM\alpha n}$ to couple to $\hat{Q}_{KM}(\alpha)$ and $\hat{Q}_{KM}(\alpha)$ respectively.

3.2.1 Isospin formalism vs. proton-neutron formalism

In the section above, we have expressed the two-body Hamiltonian in its J-representation, in which case the resulting linearized Hamiltonian will mix protons and neutrons. This is because the linearized Hamiltonian $\hat{h}_{\sigma\sigma'}$ is a linear combination of operators $\hat{\rho}_{KM}(ab)$ which has terms like $a^\dagger_p a_n$ and $a^\dagger_n a_p$. An inevitable consequence of having such terms in $\hat{h}_{\sigma\sigma'}$ is that although the total number of particles will remain the same, proton and neutron contents of the Slater determinants may change from sample to sample since

$$e^{-\beta\hat{h}_\sigma}|SD\rangle_{Z,N} = |SD'\rangle_{Z',N'}. \tag{3.45}$$

In this so called *pn-formalism*, conservation of proton and neutron numbers may be enforced, as we shall do later in Sec. 3.4.1, by projecting only those Slater determinants with the desired proton and neutron numbers. This is where the new implementation (SMMCpn) differs from the existing implementation. In the latter case, a manifest separation of the neutron and proton sectors is achieved by employing the *isospin formalism* as explained in detail in [37, 39]. An isospin invariant Hamiltonian, which is written in its JT-representation can be quadratized solely in terms of density operators that conserve proton and neutron numbers. As long as the isospin symmetry is intact, the isospin formalism should be favored because the number of auxiliary fields is halved, and instead of employing a double projection as

done in the pn-formalism to achieve the desired proton and neutron numbers, only a single projection is necessary, one for the number of protons and another for the number of neutrons, each done separately in the respective proton and neutron sectors. These factors speed up the computation noticeably. But the *raison d'existence* of the SMMCpn is not to challenge the computational efficiency of the isospin SMMC implementation, but to carry out large-scale shell-model calculations with model spaces built on non-identical proton and neutron cores, where the latter approach can definitely not be used. Improvements in computer speeds and memory have recently allowed the completion of the fp-shell calculations by the conventional diagonalization methods. Shell-model calculations in mass regions beyond the fp-shell are crucial to test model spaces to see whether configuration mixing within the set of orbitals in these valence spaces is adequate for a microscopic understanding of the nuclei in these regions. In addition, the $A \sim 100$ mass region is an important meeting point for the shell-model and approximate methods such as deformed Hartree-Fock and it is important to study interesting phenomena such as shape transitions from different perspectives. Calculations that can be carried out by SMMCpn should therefore be of great value to this end.

3.3 Monte Carlo Methods

In the sections above, we have seen how the imaginary-time evolution operator can be reduced to a multidimensional path-integral over auxiliary fields. Thus we calculate thermal expectation values by evaluating the ratio of integrals in Eqn. 3.14. In this section, we are going to review the Monte Carlo quadrature and outline the Metropolis algorithm for efficient and accurate evaluation of these multidimensional integrals. One can find more on this topic in [47, 64]. Here we will give a brief introduction.

As mentioned before, the dimensions of the integrals are of the order of $N_s^2 N_t$, and this number can be very large even for a moderate shell-model calculation. As an example, consider a typical fp-shell calculation in which proton and neutron valence spaces have 20 single-particle levels each. Remember that in the formalism we have chosen, protons and neutrons are treated alike; hence, the total number of single particle levels $N_s = N_{s\pi} + N_{s\nu}$ is 40. Using a typical value of 64 time slices, we obtain the number of auxiliary fields needed to be in the order of 10^5. Using a conventional method of integration in which we have N mesh points for each dimension of integration, we would need to evaluate the integrand N^{10^5} times, and obviously even for very small N, this would be an overwhelming number beyond the reach of any imaginable means of computation! The problem with conventional integration lies in the fact that the desired levels of accuracy can be attained in a very impractical way as a function of the number of mesh points. Take the example of an integral

evaluated using Simpson's rule, where a d-dimensional integral has an error of the order of $\mathcal{O}(\frac{1}{N^{4/d}})$. For large dimensions d, this error falls off very slowly with N. On the contrary, Monte Carlo integration treats the integral statistically where the errors in the sampling decrease with the number of samples N as $1/\sqrt{N}$, independent of the dimension of the integral. Hence, for multidimensional integrals, Monte Carlo integration has a greater advantage over standard methods, and for very large dimensions, it is the only way the integration can be carried out.

Consider the expectation value of a σ-dependent function X

$$\langle X \rangle = \frac{\int \mathcal{D}[\sigma] W(\sigma) X(\sigma)}{\int \mathcal{D}[\sigma] W(\sigma)}, \tag{3.46}$$

and assume that $W(\sigma)$ is positive-definite. (A more general case will be discussed in section 3.5.) Eqn. 3.46 can be given a statistical meaning by identifying

$$P(\sigma) = \frac{W(\sigma)}{\int \mathcal{D}[\sigma] W(\sigma)} \tag{3.47}$$

as a probability distribution satisfying

$$P(\sigma) \geq 0, \qquad \int \mathcal{D}[\sigma] P(\sigma) = 1. \tag{3.48}$$

We can approximate Eqn 3.46 by forming an average over N statistically independent samples distributed according to $P(\sigma)$

$$\langle X \rangle \approx \frac{1}{N} \sum_{\substack{i=1 \\ \sigma_i \, \epsilon \, P(\sigma)}}^{N} X(\sigma_i). \tag{3.49}$$

The value of this sum varies with the sampling. Therefore the sum itself has a probability distribution of its own. Using a central limit theorem, one can show that this distribution for large N approaches a normal distribution independent of the probability distribution $P(\sigma)$ and the function $X(\sigma)$, and the dimension d. The standard deviation in Eqn. 3.49 is given by

$$\sigma = \frac{1}{\sqrt{N}}(\langle X^2 \rangle - \langle X \rangle^2)^{1/2}, \tag{3.50}$$

where we can use the estimate

$$\langle X^2 \rangle - \langle X \rangle^2 \approx \frac{1}{N} \sum_{\substack{i=1 \\ \sigma_i \,\epsilon\, P(\sigma)}}^{N} X(\sigma_i)^2 - \Big(\frac{1}{N} \sum_{\substack{i=1 \\ \sigma_i \,\epsilon\, P(\sigma)}}^{N} X(\sigma_i) \Big)^2 \tag{3.51}$$

for large N.

We will now turn our attention to how the sampling is performed. We will do this first by considering a *Markov process* which generates a sequence of variables $\{x_1, x_2, x_3, \ldots\}$ according to a rule such that the probability distribution for the $(n+1)^{st}$ element in the sequence depends solely on the probability distribution of the n^{th} element. Such a sequence is called a *Markov chain.* Below we will show the criteria which must be satisfied by the rule to ensure that the elements in the sequence will eventually be distributed according to a specified probability distribution. Then as a specific example to this rule, we will give an outline of the commonly used Metropolis algorithm.

Let x be the current and y be the next element in a Markov chain, and let $P(x \to y)$ denote the rule by which we generate y starting from x. Since each point x is assigned to a new point y somewhere in the interval of interest, $P(x \to y)$ satisfies

$$\int \mathrm{d}y \; P(x \to y) = 1. \tag{3.52}$$

Let the probability distribution of the current element be given by normalized $p(x)$, then the probability distribution of points in the next element is given by

$$\tilde{p}(y) = \int \mathrm{d}x \; P(x \to y) p(x) \tag{3.53}$$

which obviously preserves the normalization condition, i.e., $\int \mathrm{d}y \tilde{p}(y) = 1$.

Now let $p_s(x)$ be the probability distribution that we would like to sample. Then it is sufficient for a Markov process that the rule $P(x \to y)$ satisfies the following two conditions

- one must be able to access all y with $P(x \to y)$
- the condition of *microreversibility* must be satisfied

$$p_s(x)P(x \to y) = p_s(y)P(y \to x). \tag{3.54}$$

Proof: We will first show that $p_s(x)$ is an equilibrium solution, that is, eventually after each step one gets the same probability distribution $p_s(x)$ as the one before

$$\begin{aligned} \tilde{p}(y) &= \int \mathrm{d}x\ P(x \to y)p_s(x) = \int \mathrm{d}x\ P(y \to x)p_s(y) \\ &= p_s(y) \int \mathrm{d}x\ P(y \to x) = p_s(y), \end{aligned} \tag{3.55}$$

where the condition of microreversibility and normalization were used. The second step in the proof is to show that the distribution converges to $p_s(x)$. To do this, let us first define a measure for the deviation of the distribution $p(x)$ from the equilibrium distribution $p_s(x)$ as

$$D_{old} \equiv \int \mathrm{d}x\ |p(x) - p_s(x)|. \tag{3.56}$$

The deviation in the next step will be

$$\begin{aligned} D_{new} &= \int \mathrm{d}y \left| \int \mathrm{d}x\ p(x)P(x \to y) - p_s(y) \right| \\ &= \int \mathrm{d}y \left| \int \mathrm{d}x\ (p(x) - p_s(x))P(x \to y) \right| \\ &\leq \int \mathrm{d}y \int \mathrm{d}x\ |p(x) - p_s(x)|P(x \to y), \end{aligned} \tag{3.57}$$

hence

$$D_{new} \leq \int \mathrm{d}x\ |p(x) - p_s(x)| = D_{old}. \tag{3.58}$$

Thus the deviation from the equilibrium distribution is non-increasing. The equality is satisfied only in the case of equilibrium, or in the case when some configurations are

inaccessible, but this case is excluded by hypothesis. Therefore the process is certain to yield the desired probability distribution.

There are a variety of known algorithms $P(x \to y)$ satisfying the conditions mentioned above. Because of its simplicity and applicability to an arbitrary distribution, we have used the Metropolis algorithm which is due to Metropolis, Rosenbluth, Rosenbluth, Teller, and Teller [44]. This algorithm generates field configurations $\{\sigma_1, \sigma_2, \ldots\}$ that are randomly distributed according to some probability distribution P as in Eqn. 3.47, by repeating the following procedure times

1. Start with some initial configuration σ_i
2. Move to a trial configuration σ_t
3. Calculate the ratio

$$r = \frac{P(\sigma_t)}{P(\sigma_i)} \tag{3.59}$$

4. If $r > 1$, then *accept the trial move*, i.e., $\sigma_{i+1} = \sigma_t$. If $r < 1$, then *accept the trial move with probability* r. This can be done by generating a random number R on $[0, 1]$. If $R \leq r$, then $\sigma_{i+1} = \sigma_t$, otherwise *reject the move* i.e., $\sigma_{i+1} = \sigma_i$.
5. Go to step 1.

Proof: Values σ_t can take are not restricted (see below). Hence the first condition is satisfied. To see that the condition of microreversibility is satisfied as well, consider first the case $r = P(\sigma_t)/P(\sigma_i) > 1$, for which $P(\sigma_i \to \sigma_t) = 1$. Going the other way, i.e., $\sigma_t \to \sigma_i$ is accepted with probability

$$P(\sigma_t \to \sigma_i) = \frac{P(\sigma_i)}{P(\sigma_t)} = \frac{1}{r}. \tag{3.60}$$

Therefore

$$P(\sigma_t)P(\sigma_t \to \sigma_t) = P(\sigma_i) = P(\sigma_i)P(\sigma_i \to \sigma_t). \tag{3.61}$$

The argument for the other case i.e., $r \leq 1$ follows analogously; hence, the microreversibility condition is established.

Implementation of generating trial steps: One easy way of implementing the trial move is by updating fields according to

$$\sigma_t = \sigma_i + \xi\Delta\sigma, \tag{3.62}$$

where ξ is a random number in the interval $[-1, 1]$ and $\Delta\sigma$ is the characteristic step size, which is chosen so that about half of the trial steps are accepted. To see why, consider the case in which the step size is very large; then, it is very likely that $P(\sigma_t)$ will be much smaller than $P(\sigma_i)$; thus, the step will be rejected. In the other extreme case, in which the step size is very small, the step is very likely to be accepted, but then σ will take a very long time to explore the full space. Therefore the step size should be chosen so that a compromise between the two inefficient cases is obtained.

An alternative way of updating the fields turns out to be more efficient due to a considerable reduction in the correlation length (discussed below). This is achieved by employing a discrete version of the HS transformation:

$$e^{-\frac{1}{2}\Delta\beta\lambda\hat{O}^2} \approx \int \mathrm{d}\sigma \; f(\sigma) e^{-\Delta\beta s\sigma\lambda\hat{O}} + \mathcal{O}(\Delta\beta^3), \tag{3.63}$$

where

$$f(\sigma) = \frac{1}{6}[\delta(\sigma - \sigma_0) + \delta(\sigma + \sigma_0) + 4\delta(\sigma)], \tag{3.64}$$

and $\sigma_0 = (3/\lambda\Delta\beta)^{1/2}$. Using this procedure, the path integral has been reduced to a path sum in which the fields have become three-way variables. Note that this approach, which can be called the discrete evolution, would not introduce a loss of accuracy, because the accuracy of the HS transformation is determined by the commutator terms (remember that Eqn. 3.3 is valid up to order $\Delta\beta^2$). In the implementation of this approach, we choose a pre-determined relative probability η. Then for each field σ, we generate a random number ξ in $[0, 1]$. If $\xi \leq \eta$, then the field is allowed to take one of the three permissible values according to their relative weight, i.e.,

$$\sigma_t = \begin{cases} \sigma_0 & \text{(with 1/6 probability)} \\ 0 & \text{(with 2/3 probability)} \\ -\sigma_0 & \text{(with 1/6 probability).} \end{cases} \tag{3.65}$$

Just like in the alternative implementation mentioned above, the relative probability η is chosen so that the acceptance ratio is $\approx 50\%$. The SMMCpn code uses this approach.

Thermalization and decorrelation: We start our calculations with randomly initiated auxiliary fields. In order to ensure that the fields get distributed according to the sampling function, the Metropolis algorithm must be run long enough. This

process is known as *thermalization*. Only after stabilizing the walkers density at the sampling density, we must start the actual sampling of the observables.

Another point of importance in the sampling is statistical independence. Since the generation of $(i+1)$th configuration depends on the ith one, we should expect some correlation between successive samples. The error estimates given by Eqn. 3.50 would then be wrong, since in its derivation, statistical independence of the samples $X(\sigma_i)$ is assumed. As a measure of correlation of $X(\sigma_i)$ to $X(\sigma_{i+k})$, one can use the autocorrelation function,

$$C(k) = \frac{\langle X_i X_{i+k} \rangle - \langle X_i \rangle^2}{\langle X_i^2 \rangle - \langle X_i \rangle^2}. \tag{3.66}$$

Once the autocorrelations are obtained for various correlation lengths k, one can choose a particular value of correlation leg at which autocorrelation function is small enough, say, about 0.1. Then we will skip the field configurations σ_i as many times as this length to sample observables $X(\sigma_i)$. This way we can practically render the sampling statistically independent.

3.4 Calculation of Static Observables

Having reviewed how the integration is carried out, we now turn our attention to the evaluation of the integrands, in particular the various traces appearing in Eqn. 3.12. This task can be handled by the algebra of $N_s \times N_s$ matrices. This follows from the matrix representation of $\hat{h}_\sigma$ (Eqn. 3.10), and thus of $\hat{U}_\sigma$. Introducing the matrix notation, we define $(\mathbf{h}_\sigma)_{\alpha\beta} = \langle \alpha | \hat{h}_\sigma | \beta \rangle$. Then we can write $\mathbf{u}_\sigma(\tau_n) = e^{-\Delta\beta \mathbf{h}_\sigma(\tau_n)}$ and express the one-body evolution operator in its matrix representation as

$$\mathbf{U}_\sigma = \mathbf{u}_\sigma(\tau_{N_t}) \ldots \mathbf{u}_\sigma(\tau_2)\mathbf{u}_\sigma(\tau_1). \tag{3.67}$$

For the evaluation of thermal expectation values, one can use either the grand canonical or the canonical ensembles. The former is not a suitable choice for atomic nuclei because of fluctuations in particle number, and the fact that expectation values of observables are averaged over neighboring nuclei, which often display dramatically different properties. Therefore a canonical ensemble must be employed. In our calculations, we will use the Fourier extraction method [37, 50] to retrieve the canonical traces from the grand canonical counterparts.

We will start with evaluating $\mathrm{Tr}\hat{U}_\sigma$ for 1-body, 2-body, ... N_s-body states

$$\begin{aligned}
\mathrm{Tr}_0\hat{U}_\sigma &= \langle \mathbf{0}|\hat{U}_\sigma|\mathbf{0}\rangle = 1, \\
\mathrm{Tr}_1\hat{U}_\sigma &= \sum_i \langle i|\hat{U}_\sigma|i\rangle = \mathrm{tr}\mathbf{U}_\sigma, \\
\mathrm{Tr}_2\hat{U}_\sigma &= \frac{1}{2}\sum_{ij}\langle ij|\hat{U}_\sigma|ij\rangle = \frac{1}{2}\left[(\mathrm{tr}\mathbf{U}_\sigma)^2 - \mathrm{tr}\mathbf{U}_\sigma^2\right], \\
&\vdots \\
\mathrm{Tr}_{N_s}\hat{U}_\sigma &= \det\mathbf{U}_\sigma.
\end{aligned} \tag{3.68}$$

Summing up the n-body traces corresponding to all possible number of nucleons the valence space can get hold of, we obtain the grand canonical result,

$$\xi = \mathrm{Tr}\hat{U}_\sigma = \det(\mathbf{1} + \mathbf{U}_\sigma). \tag{3.69}$$

This relationship can be verified by a direct expansion of the determinant in powers of $\mathbf{U}$. Above, the labels Tr and tr are used for many-body operator and matrix traces respectively. The vacuum state is denoted by $|\mathbf{0}\rangle$. A corresponding canonical trace for fixed N and Z,

$$\xi_{\mathcal{A}} = \mathrm{Tr}_{\mathcal{A}}\hat{U}_\sigma = \mathrm{Tr}\,\hat{P}_{\mathcal{A}}\hat{U}_\sigma \tag{3.70}$$

will be extracted in the next section. Above $\mathcal{A} \equiv (N, Z) = (A, T_z)$ is a shorthand notation characterizing a specific nuclei for which the canonical trace can be obtained by using the projection operators for the good A and T_z:

$$\hat{P}_{\mathcal{A}} = \hat{P}_A\hat{P}_{T_z} = \delta(\hat{N} - A)\,\delta(\hat{T}_z - T_z). \tag{3.71}$$

3.4.1 Projecting onto good A and T_z states

The evaluation of thermal expectation values of an observable $\hat{X}$ (we will consider one and two-body cases below) for a given nucleus specified by $\mathcal{A}$,

$$\langle\hat{X}\rangle_{\mathcal{A}} = \frac{\int \mathcal{D}[\sigma]\,W(\sigma)\langle\hat{X}\rangle_{\sigma,\mathcal{A}}\Phi(\sigma)}{\int \mathcal{D}[\sigma]\,W(\sigma)\Phi(\sigma)}, \tag{3.72}$$

involves the computation of the traces in

$$\langle \hat{X} \rangle_{\sigma,\mathcal{A}} = \frac{\mathrm{Tr}_{\mathcal{A}}[\hat{U}_\sigma \hat{X}]}{\zeta_{\mathcal{A}}}. \tag{3.73}$$

Let us start with the evaluation of $\zeta_{\mathcal{A}}$. We first write the (total) number-projection operator in its familiar integral representation

$$\hat{P}_A = \int_0^{2\pi} \frac{d\phi}{2\pi} e^{-i\phi A} e^{i\phi \hat{N}}. \tag{3.74}$$

However, we prefer to use the equivalent expression

$$\hat{P}_A = e^{-\beta\mu A} \int_0^{2\pi} \frac{d\phi}{2\pi} e^{-i\phi A} e^{(\beta\mu + i\phi)\hat{N}}, \tag{3.75}$$

in which an arbitrary constant μ is introduced. A numerical value for this constant is chosen to ensure better numerical stability. The canonical trace over a fixed number of nucleons can thus be written as

$$\begin{aligned} \zeta_A &= \mathrm{Tr}\,(e^{-\beta\mu A} \int_0^{2\pi} \frac{d\phi}{2\pi} e^{-i\phi A} e^{(\beta\mu + i\phi)\hat{N}} \hat{U}_\sigma) \\ &= e^{-\beta\mu A} \int_0^{2\pi} \frac{d\phi}{2\pi} e^{-i\phi A} \mathrm{Tr}\, e^{(\beta\mu + i\phi)\hat{N}} \hat{U}_\sigma \\ &= e^{-\beta\mu A} \int_0^{2\pi} \frac{d\phi}{2\pi} e^{-i\phi A} \det(1 + e^{\beta\mu} e^{i\phi} \mathbf{U}_\sigma), \end{aligned} \tag{3.76}$$

where the linearity property of a trace is used in the second line. Upon diagonalizing $\mathbf{U}_\sigma$ and writing its N_s eigenvalues (which can, in general, be complex) in the form $e^{-\epsilon_\lambda}$, the trace above can also be expressed as

$$\zeta_A = e^{-\beta\mu A} \int_0^{2\pi} \frac{d\phi}{2\pi} e^{-i\phi A} \prod_\lambda (1 + e^{i\phi} e^{\beta(\mu - \epsilon_\lambda)}). \tag{3.77}$$

The grand canonical trace in the integrand of Eqn. 3.77 contains contributions from canonical ensembles of all particle numbers in $0 \leq A \leq N_s$. Since these contributions vary noticeably with A, the value of μ is optimally chosen so that the contribution corresponding to the desired value of A can be obtained with higher accuracy. This can be done by following the analogy of obtaining the chemical potential

μ in thermodynamics. First we sort the eigenvalues of $\mathbf{U}_\sigma$ in increasing order so that $\mathrm{Re}\,\epsilon_1 \leq \mathrm{Re}\,\epsilon_2 \leq \ldots \mathrm{Re}\,\epsilon_{N_s}$. A good choice for μ is then $(\mathrm{Re}\,\epsilon_A + \mathrm{Re}\,\epsilon_{A+1})/2$ [37].

In order to target a specific nucleus in our calculations, we also need to project onto good T_z states. This is done by the application of (total) T_z-projection operator as well:

$$\begin{aligned} \zeta_{\mathcal{A}} &= e^{-\beta\mu A}\int_0^{2\pi}\frac{d\phi}{2\pi}\int_0^{2\pi}\frac{d\theta}{2\pi}e^{-i\phi A}e^{-i\theta T_z}\mathrm{Tr}\left[e^{(\beta\mu+i\phi)\hat{N}}e^{i\theta\hat{T}_z}\hat{U}_\sigma\right] \\ &= e^{-\beta\mu A}\int_0^{2\pi}\frac{d\phi}{2\pi}\int_0^{2\pi}\frac{d\theta}{2\pi}e^{-i\phi A}e^{-i\theta T_z}\det(1+e^{\beta\mu+i\phi}e^{i\theta\mathbf{T_z}}\mathbf{U}_\sigma), \end{aligned} \tag{3.78}$$

where $\mathbf{T_z}$ is given by

$$\mathbf{T_z} = \frac{1}{2}\left(\begin{array}{c|c} \mathbf{-1} & \mathbf{0} \\ \hline \mathbf{0} & \mathbf{1} \end{array}\right). \tag{3.79}$$

Above the upper left (lower right) quadrant is the proton (neutron) sector.

When implementing the Fourier extraction method, discrete sums are used instead of the integrals above. This is done by the replacement

$$\int_0^{2\pi}\frac{d\phi}{2\pi}\int_0^{2\pi}\frac{d\theta}{2\pi} \longrightarrow \frac{1}{N_s(N_{T_z}+1)}\sum_{m=1}^{N_s}\sum_{n=0}^{N_{T_z}}, \tag{3.80}$$

where the quadrature points are given by $\phi_m = 2\pi m/N_s$ and $\theta_n = 2\pi n/(N_{T_z}+1)$, where N_s is the number of single-particle states, and N_{T_z} is the number of values T_z can take, which can be determined simply from the number of nucleons and the the orbitals in the valence space.

Now we consider the evaluation of the expectation values of one- and two-body operators $\hat{X}$. Starting with the one-body case first, in each Monte Carlo sample we need to compute

$$\langle\hat{X}\rangle_{\sigma,\mathcal{A}} = \sum_{\alpha\beta}\mathbf{X}_{\alpha\beta}\langle a_\alpha^\dagger a_\beta\rangle_{\sigma,\mathcal{A}}, \tag{3.81}$$

where $\mathbf{X}_{\alpha\beta} = \langle\alpha|\hat{X}|\beta\rangle$. Hence the basic quantity of interest is $\langle a_\alpha^\dagger a_\beta\rangle_{\sigma,\mathcal{A}}$, which can be obtained using the projection techniques that are described above on the grand canonical counterpart [50]:

$$\langle a_\alpha^\dagger a_\beta \rangle_\sigma = [(1+\mathbf{U}_\sigma)^{-1}\mathbf{U}_\sigma]_{\beta\alpha}. \tag{3.82}$$

Hence we have

$$\langle a_\alpha^\dagger a_\beta \rangle_{\sigma,\mathcal{A}} = \frac{1}{N_s(N_{T_z}+1)\zeta_{\mathcal{A}}(\sigma)} \sum_{m=1}^{A}\sum_{n=0}^{N_{T_z}} e^{-iA\phi_m} e^{-\beta A\mu} e^{-iT_z\theta_n} \eta_{mn}(\sigma)\gamma_{\alpha\beta}^{mn}(\sigma), \tag{3.83}$$

where $\eta_{mn}(\sigma)$ and $\gamma_{\alpha\beta}^{mn}(\sigma)$ are defined as

$$\eta_{mn}(\sigma) = \det[1 + e^{\beta\mu} e^{i\phi_m} e^{i\theta_n \mathbf{T_z}} \mathbf{U}_\sigma], \tag{3.84}$$

$$\gamma_{\alpha\beta}^{mn}(\sigma) = [(1 + e^{\beta\mu} e^{i\phi_m} e^{i\theta_n \mathbf{T_z}} \mathbf{U}_\sigma)^{-1} e^{\beta\mu} e^{i\phi_m} e^{i\theta_n \mathbf{T_z}} \mathbf{U}_\sigma]_{\beta\alpha}. \tag{3.85}$$

A similar expression can be written for the expectation values of two-body operators. For this purpose, we first rearrange the creation and annihilation operators

$$\begin{aligned} \langle \hat{X} \rangle_{\sigma,\mathcal{A}} &= \frac{1}{4} \sum_{\alpha\beta\gamma\delta} \mathbf{X}_{\alpha\beta\gamma\delta} \langle a_\alpha^\dagger a_\beta^\dagger a_\delta a_\gamma \rangle_{\sigma,\mathcal{A}} \\ &= -\frac{1}{4} \sum_{\alpha\beta\gamma\delta} \mathbf{X}_{\alpha\beta\gamma\delta} \langle a_\alpha^\dagger a_\delta a_\beta^\dagger a_\gamma \rangle_{\sigma,\mathcal{A}} + \frac{1}{4} \sum_{\alpha\beta\gamma} \mathbf{X}_{\alpha\beta\gamma\beta} \langle a_\alpha^\dagger a_\gamma \rangle_{\sigma,\mathcal{A}}, \end{aligned} \tag{3.86}$$

where $\mathbf{X}_{\alpha\beta\gamma\delta} = \langle \alpha\beta | \hat{X} | \gamma\delta \rangle$. The first term can be evaluated using $\langle a_\alpha^\dagger a_\delta a_\beta^\dagger a_\gamma \rangle_{\sigma,\mathcal{A}}$ which is given by

$$\begin{aligned} \langle a_\alpha^\dagger a_\beta a_\gamma^\dagger a_\delta \rangle_{\sigma,\mathcal{A}} &= \frac{1}{N_s(N_{T_z}+1)\zeta_{\mathcal{A}}(\sigma)} \sum_{m=1}^{A}\sum_{n=0}^{N_{T_z}} e^{-iA\phi_m} e^{-\beta A\mu} e^{-iT_z\theta_n} \times \\ &\quad \times \eta_{mn}(\sigma)[\gamma_{\alpha\beta}^{mn}(\sigma)\gamma_{\gamma\delta}^{mn}(\sigma) - \gamma_{\alpha\delta}^{mn}(\sigma)\gamma_{\gamma\beta}^{mn}(\sigma) + \delta_{\beta\gamma}\gamma_{\alpha\delta}^{mn}(\sigma)] \end{aligned} \tag{3.87}$$

Computational effort for the calculation of η_{mn} can be eased by the diagonalization of $\tilde{\mathbf{U}}_\sigma$ which is defined as

$$\tilde{\mathbf{U}}_\sigma^{(n)} \equiv e^{i\theta_n \mathbf{T_z}} \mathbf{U}_\sigma = [\cos(\frac{\theta_n}{2})\mathbf{1} + i\sin(\frac{\theta_n}{2})2\mathbf{T_z}]\ \mathbf{U}_\sigma. \tag{3.88}$$

Thus, we can express the determinant in terms of the eigenvalues $\lambda_i^{(n)}$ of $\tilde{\mathbf{U}}_\sigma^{(n)}$

$$\eta_{mn}(\sigma) = \prod_i^{N_s}(1 + e^{\beta\mu}e^{i\phi_m}\lambda_i^{(n)}). \tag{3.89}$$

The transformation matrix $\mathcal{P}$ associated with $\tilde{\mathbf{U}}_\sigma^{(n)}$ can then be used for the evaluation of $\gamma_{\alpha\beta}^{mn}(\sigma)$ as well:

$$\gamma_{\alpha\beta}^{mn}(\sigma) = \sum_\delta \mathcal{P}_{\beta\delta}(1 + e^{\beta\mu}e^{i\phi_m}\lambda_\delta^{(n)})^{-1}e^{\beta\mu}e^{i\phi_m}\mathcal{P}_{\delta\alpha}^{-1}. \tag{3.90}$$

3.4.2 Projecting onto good parity states

An important property of nuclear levels is parity. Parity distribution of nuclear levels is important for understanding parity-violating processes and neutron capture reactions. Many heavy elements are synthesized by radiative capture of neutrons by s- and r-processes, and knowledge of parity-projected level densities is crucial for theoretical estimation of the nuclear reaction rates in nucleosynthesis. Using similar projection techniques presented in the section above, it is also possible to project onto good parity states in the evaluation of the traces. Since calculation of level densities in the shell model is computationally intensive due to large model spaces, SMMC methods were used in the past for this purpose [3,45]. Here we will follow the discussion given in [45].

First, we define positive and negative parity projection operators

$$\hat{P}_\pm = (1 \pm \hat{P})/2, \tag{3.91}$$

where $\hat{P}$ is the parity operator. In its matrix representation, $\mathbf{P}$ is diagonal with matrix elements $(-1)^{l_i}$, where l_i is the orbital angular momentum of the single-particle level i. Thermal expectation values of an observable over good parity states is given by

$$\begin{aligned}\langle\hat{X}\rangle_{\pm} &= \frac{\mathrm{Tr}[\hat{P}_{\pm}\hat{U}\hat{X}]}{\mathrm{Tr}[\hat{P}_{\pm}\hat{U}]} \\ &= \frac{\int \mathcal{D}[\sigma]\, G(\sigma)\mathrm{Tr}_{\mathcal{A}}[\hat{P}_{\pm}\hat{U}_{\sigma}\hat{X}]}{\int \mathcal{D}[\sigma]\, G(\sigma)\mathrm{Tr}_{\mathcal{A}}[\hat{P}_{\pm}\hat{U}_{\sigma}]}\end{aligned} \tag{3.92}$$

which can be rewritten as

$$\langle\hat{X}\rangle_{\pm} = \frac{\int \mathcal{D}[\sigma]\, W(\sigma)\Phi(\sigma)[\langle\hat{X}\rangle_{\sigma,\mathcal{A}} \pm \langle\hat{X}\rangle_{\sigma,\mathcal{A},P}\zeta_{\mathcal{A},P}(\sigma)/\zeta_{\mathcal{A}}(\sigma)]}{\int \mathcal{D}[\sigma]\, W(\sigma)\Phi(\sigma)[1 \pm \zeta_{\mathcal{A},P}(\sigma)/\zeta_{\mathcal{A}}(\sigma)]}. \tag{3.93}$$

Above we have used the definition of the canonical partition function of the non-interacting propagator $\zeta_{\mathcal{A}}(\sigma)$, expectation value of $\hat{X}$ in the non-interacting system $\langle\hat{X}\rangle_{\sigma,\mathcal{A}}$, and the Monte Carlo weight function $W(\sigma)$ as given in Sec. 3.1, and introduced new quantities

$$\zeta_{\mathcal{A},P}(\sigma) \equiv \mathrm{Tr}_{\mathcal{A}}[\hat{P}\hat{U}_{\sigma}], \tag{3.94}$$

$$\langle\hat{X}\rangle_{\sigma,\mathcal{A},P} = \frac{\mathrm{Tr}_{\mathcal{A}}[\hat{P}\hat{U}_{\sigma}\hat{X}]}{\mathrm{Tr}_{\mathcal{A}}[\hat{P}\hat{U}_{\sigma}]}. \tag{3.95}$$

The operator $\hat{P}\hat{U}_{\sigma}$ can be represented by the matrix $\mathbf{PU}_{\sigma}$, and using the matrix algebra quantities like $\zeta_{\mathcal{A},P}(\sigma)$ and $\langle\hat{X}\rangle_{\sigma,\mathcal{A},P}$ are computed as usual with the difference that the matrix U_{σ} is replaced by $\mathbf{PU}_{\sigma}$.

3.5 The Monte Carlo Sign Problem

The whole discussion of the SMMC method relies on the evaluation of the path-integrals stochastically. For this purpose, as mentioned in section 3.3, the weight function $W(\sigma)$ must be positive-definite for all σ in order to interpret it as a probability distribution. However this is not always the case. Apart from a class of schematic interactions [39], most interactions produce $\mathrm{Tr}\hat{U}_{\sigma}$; hence, $W(\sigma)$ is not necessarily positive-definite. In that case, the average value of the sign, $\langle\Phi_{\sigma}\rangle_W$, which is used in the normalization of Eqn. 3.46, approaches zero due to cancellations of the fluctuating sign from sample to sample. As a result, the uncertainity in Monte Carlo estimates in Eqn. 3.18 becomes too large. This situation causes uncontrollable numerical instabilities, and is known as the Monte Carlo "sign" problem. The sign problem

often gets worse at lower temperatures due to an exponential decrease in the average value of the sign with β, and thus limits the usefulness of the method most severely at the ground-state calculations. It turns out that the sign problem is inherent to all fermionic Monte Carlo methods [42], and an exact cure is still not known although it is possible to delay the problem [59]. In this section, we are going to discuss the issue of the sign problem at some length and finally outline a practical solution method due to Alhassid *et.al.* [2], which is used in the Zr and Mo calculations that will be presented later in this work. In the literature there exist numerous (isospin) SMMC studies in which the use of this technique has been validated [18, 37, 39, 40].

An apprehension of the sign problem is closely related to the time-reversal properties of the linearized Hamiltonian. The time-reversed partners of the creation and annihilation operators are defined as:

$$\begin{aligned} \bar{a}_{jm} &\equiv a_{j\bar{m}} = (-1)^{j+m} a_{jm}, \\ \bar{a}^{\dagger}_{jm} &\equiv a^{\dagger}_{j\bar{m}} = (-1)^{j+m} a^{\dagger}_{jm}. \end{aligned} \tag{3.96}$$

Note that the spin-half nature of the states implies

$$\bar{a}_{jm} = -a_{jm}, \qquad \bar{\bar{a}}^{\dagger}_{jm} = -a^{\dagger}_{jm}. \tag{3.97}$$

Let us write a given Hamiltonian in an explicit time-reversal invariant form

$$\hat{H} = \sum_i \epsilon_i a^{\dagger}_i a_i + \frac{1}{2} \sum_{\alpha} \lambda_{\alpha} \{\hat{\rho}_{\alpha}, \hat{\bar{\rho}}_{\alpha}\}, \tag{3.98}$$

where all λ_{α} are real and the density operators are given by

$$\hat{\rho}_{\alpha} = \sum_{ij} C^{\alpha}_{ij} \hat{\rho}_{ij}, \tag{3.99}$$

and $\hat{\bar{\rho}}_{\alpha}$ is the time-reverse of $\hat{\rho}_{\alpha}$. Applying the HS transformation, we obtain the linearized Hamiltonian

$$\hat{h}_{\sigma}(\tau_n) = \sum_i \epsilon_{\alpha} a^{\dagger}_i a_i + \sum_{\alpha} (s_{\alpha} \lambda_{\alpha} \sigma_{\alpha n} \hat{\rho}_{\alpha} + s_{\alpha} \lambda_{\alpha} \sigma^{*}_{\alpha n} \hat{\bar{\rho}}_{\alpha}). \tag{3.100}$$

Note that $\hat{\rho}_{\alpha}$ and $\hat{\bar{\rho}}_{\alpha}$ couple to complex-conjugate fields, but the linearized Hamiltonian is not necessarily time-reversal symmetric in general. However for the class

of Hamiltonians with λ_α negative for all α, we have $s_\alpha = 1$ and the time-reversal symmetry is established,

$$\hat{\bar{h}}_\sigma = \hat{h}_\sigma. \tag{3.101}$$

We will now show that this property will guarantee that the grand-canonical $\mathrm{Tr}\hat{U}_\sigma$ be positive-definite and thus the sign be equal to unity for all samples. Let us start with reordering the single-particle states such that their vector representation contains states with $m > 0$ in the first half, and their time-reversal partners in the other:

$$\begin{pmatrix} jm \\ j\bar{m} \end{pmatrix}. \tag{3.102}$$

Then one can show that, in its matrix representation, $\hat{h}$ can then be written as

$$\mathbf{h}_n = \begin{pmatrix} \mathbf{A}_n & \mathbf{B}_n \\ -\mathbf{B}_n^* & \mathbf{A}_n^* \end{pmatrix}. \tag{3.103}$$

It then follows that the one-body imaginary-time evolution operator will be represented by

$$\mathbf{U} = \prod_n e^{-\Delta\beta \mathbf{h}_n} = \begin{pmatrix} \mathbf{P} & \mathbf{Q} \\ -\mathbf{Q}^* & \mathbf{P}^* \end{pmatrix}. \tag{3.104}$$

The matrices $\mathbf{A}_n$,$\mathbf{B}_n$,$\mathbf{P}$,$\mathbf{Q}$ are of dimension $N_s/2$. Diagonalization of $\mathbf{U}$ then yields a complex-conjugate pair of eigenvalues, ϵ and ϵ^*, with the eigenvectors $\begin{pmatrix} u \\ v \end{pmatrix}$ and $\begin{pmatrix} -v^* \\ u^* \end{pmatrix}$, respectively. Thus we have

$$\mathrm{Tr}\hat{U} = \det\left[\mathbf{1} + \mathbf{U}\right] = \prod_\lambda^{N_s/2} (1 + \epsilon_\lambda)(1 + \epsilon_\lambda^*) > 0. \tag{3.105}$$

For the more complicated canonical case, in which the trace above includes only states of fixed particles, $\mathrm{Tr}\hat{U}$ is also positive-definite for even-even nuclei under the condition of $\lambda_\alpha < 0$. However, it can be shown that there is another kind of sign problem for odd-A nuclei. The discussion below is taken from Koonin *et. al.* [37].

For demonstrating the point, only one kind of nucleon in the simple cases in which $N_s = 2$ and $A = 1$ or $A = 2$ is considered. It follows from the Eqn. 3.77 in its N_s-point quadrature form that

$$\begin{aligned} \zeta_A &= \frac{1}{2}\sum_{m=1}^{2} e^{-i\phi_m A}\prod_{\lambda=1}^{2}[1 + e^{i\phi_m}e^{-\beta\epsilon_\lambda}] \\ &= \frac{1}{2}\sum_{m=1}^{2}\{e^{-i\phi_m A} + e^{-i\phi_m(A-2)}e^{-\beta \mathrm{Re}\ \epsilon_1} + e^{i\phi_m(A-1)}\mathrm{Re}\ e^{-\beta\epsilon_1}\}, \end{aligned} \tag{3.106}$$

where the $e^{-\beta\mu}$ term is dropped for the sake of simplicity. It can be shown that when the sum is evaluated, the first two terms survive in the case of $A = 2$. Since these terms are positive-definite, so is ζ_A. In the odd case of $A = 1$, the surviving term is the last one, which is real but not positive-definite.

The condition that λ_α is negative (positive) for good (bad) sign was established for the Hamiltonian expressed in the form of Eqn. 3.98. The equivalent sign rule for a Hamiltonian, which is specified in the form (Eqn 3.40), follows from

$$\hat{H}_2' = \frac{1}{2}\sum_{K\alpha}(-1)^K \lambda_{K\alpha}\sum_M \hat{\rho}_{KM}(\alpha)\hat{\bar{\rho}}_{KM}(\alpha), \tag{3.107}$$

where we have used the time-reverse of a given density operator $\hat{\rho}_{KM}(\alpha)$,

$$\hat{\bar{\rho}}_{KM}(\alpha) = (-1)^{K+M}\hat{\rho}_{K-M}(\alpha). \tag{3.108}$$

Thus we get the sign rule by which the condition of negative coupling constant can be checked:

$$\mathrm{sgn}(\lambda_{K\alpha}) = (-1)^{K+1}. \tag{3.109}$$

Shell-model applications using valence spaces with orbitals of mixed parity, such as the Zr and Mo calculations (Sec. 4.2), require the inclusion of parity in the arguments above. In that case, the matrix elements $E_{K\pi}(ac, bd)$ of good parity $\pi = (-1)^{l_a+l_c} = (-1)^{l_b+l_d}$ are constructed from the two-body interaction matrix elements $V_{J\bar{\pi}}(ab, cd)$ of good parity $\bar{\pi} = (-1)^{l_a+l_b} = (-1)^{l_c+l_d}$. (Note that any set of orbitals abcd that conserves $\bar{\pi}$ also conserves π.) Then diagonalization of the matrices $E_{K\pi}$ produce eigenvalues $\lambda_{K\pi\alpha}$ and eigenvectors $v_{K\pi\alpha}$. In the Condon-Shortley convention [17]

$\hat{\tilde{\rho}}_{KM}(\alpha) = \pi(-1)^{K+M}\hat{\rho}_{K-M}(\alpha)$, and now the modified sign rule gives the "good" eigenvalues by:

$$\mathrm{sgn}(\lambda_{K\pi\alpha}) = \pi(-1)^{K+1}. \tag{3.110}$$

3.5.1 A practical solution to the sign problem

Realistic Hamiltonians expressed in the form of Eqn. 3.107 do not necessarily have all $\lambda_{K\pi\alpha}$ satisfying the sign rule of Eqn. 3.110. The practical solution to the sign problem presented in [2] is based on the idea of identifying the "good" and "bad" parts of a given Hamiltonian and constructing a "nearby" family of Hamiltonians which gives good sign and depends on a continuous coupling parameter g. Observables of interest are then extrapolated to the physical value of g.

A given Hamiltonian can be decomposed into its "good" and "bad" parts as

$$\begin{aligned} \hat{H}_G &= \sum_i \epsilon_i a_i^\dagger a_i + \frac{1}{2}\sum_{\lambda_\alpha<0} \lambda_\alpha\{\hat{\rho}_\alpha, \hat{\tilde{\rho}}_\alpha\}, \\ \hat{H}_B &= \frac{1}{2}\sum_{\lambda_\alpha>0} \lambda_\alpha\{\hat{\rho}_\alpha, \hat{\tilde{\rho}}_\alpha\}, \end{aligned} \tag{3.111}$$

where $\hat{H}_G$ contains the one-body part plus the two-body terms producing good sign, while $\hat{H}_B$ consists of the remaining two-body terms.

A family of Hamiltonians is then constructed

$$H_g = f(g)H_G + gH_B \tag{3.112}$$

where $f(g)$ is a smooth function with $f(g < 0) > 0$ so that for negative values of the continuous parameter g, the Hamiltonian 3.112 satisfies good-sign properties. Furthermore f is chosen to satisfy $\hat{H}_{g=1} = \hat{H}$ so that we obtain back the original Hamiltonian at $g = 1$ where we will extrapolate. The arbitrariness in $f(g)$ other than the restrictions above can be used to have a handle on the smoothness of the extrapolations, if need be. For all the SMMCpn calculations reported in this work $f(g) = 1$ is used conveniently.

Since the new Hamiltonian produces $\Phi_\sigma = 1$ for $g \leq 0$ by construction, we can calculate

$$\langle\hat{O}\rangle_g = \frac{\mathrm{Tr}[\hat{O}e^{-\beta\hat{H}_g}]}{\mathrm{Tr}[e^{-\beta\hat{H}_g}]} \tag{3.113}$$

accurately and if $\langle \hat{O} \rangle_g$ is a smooth function of g, we should be able to extrapolate it to $g = 1$. In practice, we fit to polynomials $\sum_{i=0}^{n} a_i (g-1)^i$ by a linear least-square method. The degree of the polynomial is chosen to be the lowest giving $\chi^2 \approx 1$ per datum.

In our calculations, linear, or at most quadratic extrapolations have been used for all the observables except energy for which a cubic polynomial has been chosen. For the latter case, a constrained fit is used such that

$$\left. \frac{d\langle H \rangle_g}{dg} \right|_{g=1} = 0, \tag{3.114}$$

due to the variational principle. Note that the variational condition holds true only for ground-state calculations ($\beta \to \infty$), and should one wish to perform finite temperature calculations, a variation-free energy method can be used [49].

Fig. 3.1 shows the extrapolation technique for various ground-state observables of ^{48}Ti. Monte Carlo calculations for each of the six data points from $g = -1$ to $g = 0$ were carried out at $\beta = 2$ MeV^{-1} using $N_t = 128$ time steps, and 9600 uncorrelated samples. The definitions of the observables are given in Sec. 4.1.

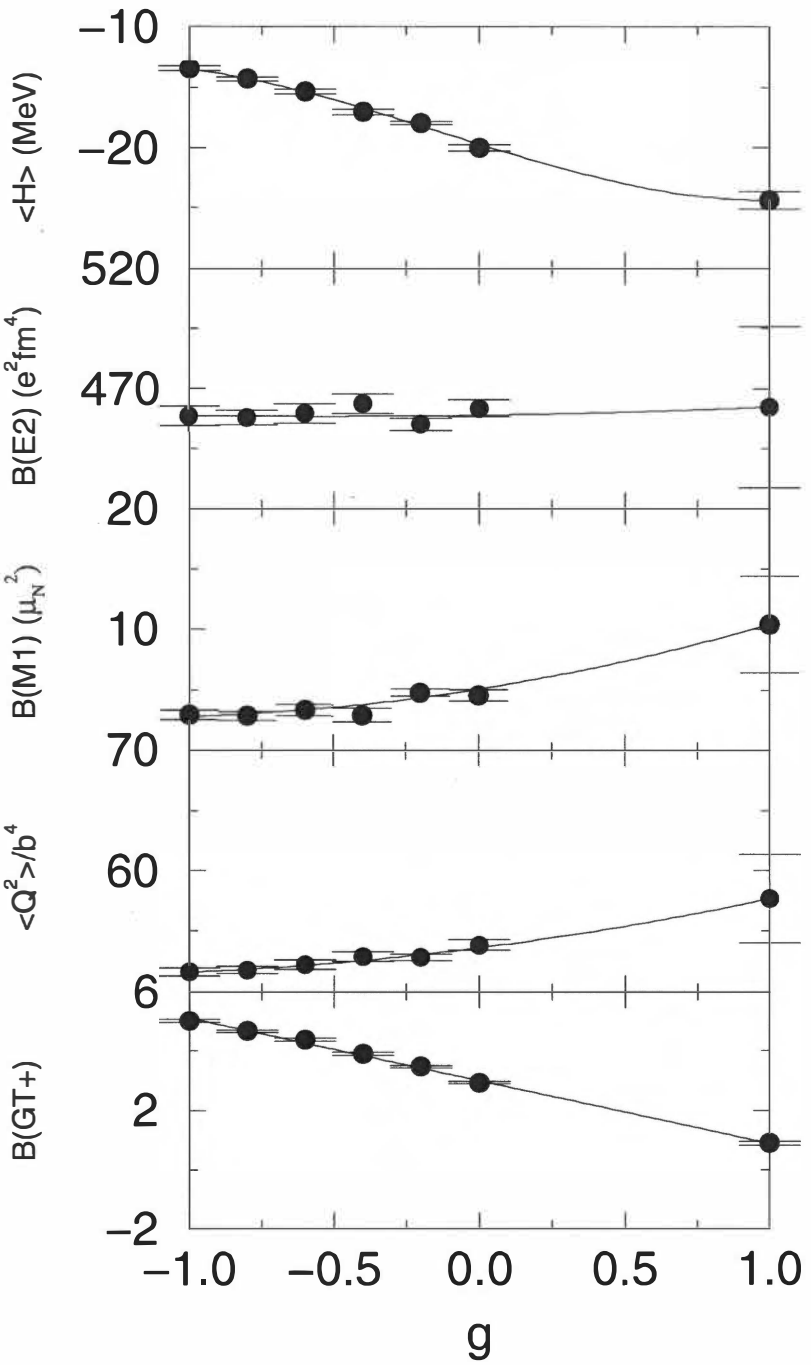


Figure 3.1: Extrapolation of some observables for ^{48}Ti

Chapter 4

Numerical Results

4.1 Test Cases

The purpose of this section is to benchmark the accuracy of the new implementation by comparing numerical results of the SMMCpn approach with those obtained by exact diagonalization and earlier isospin SMMC methods. We will do this in two steps. First, we will compare the ground-state energies of a few *sd*-shell nuclei against ANTOINE results using schematic interactions. The reason for using such interactions is that they are free of the sign problem, and SMMC calculations do not pertain to the extrapolation method. The interactions are created purely for testing purposes and results are not physically relevant.

The first set of the *sd*-shell calculations were performed using a quadrupole interaction given by

$$\hat{V} = -\chi \hat{Q} \cdot \hat{Q} \tag{4.1}$$

where the operator $\hat{Q}$ is defined as

$$\hat{Q} = \frac{1}{\sqrt{5}} \sum_{ab} \langle j_a || \frac{dV_{WS}}{dr} Y_2 || j_b \rangle [a^\dagger_{j_a} \otimes \tilde{a}_{j_b}]^{J=1,T=0}. \tag{4.2}$$

The term V_{WS} in the equation above is the central part of a Woods-Saxon potential with parameters given in [7]. We chose $\chi = 0.0260$ MeV^{-1}fm^2 for the interaction strength, and for either kind of nucleons, we adopted the same single-particle energies as the *sd*-shell calculations with the USD-interaction. Note that, since the interaction lacks a pairing term, in order to obtain the ground-state energies, we need to "cool

Table 4.1: Comparison of the ground-state energies (in MeV), as calculated by SMMCpn and the ANTOINE results. A quadrupole interaction is used.

Nucleus	E (ANTOINE)	E (SMMCpn)
^{24}Mg	-36.60	-36.37 ± 0.05
^{26}Mg	-40.61	-40.43 ± 0.05
^{22}Ne	-28.22	-28.01 ± 0.03
^{28}Si	-45.98	-45.73 ± 0.04

down" the system at a high value of β. For this purpose, $\beta = 4$ MeV^{-1} was used. A comparison of the results is given in Table 4.1.

A second set of calculations was performed for the same nuclei, this time, by adding a pairing term to the interaction used in the previous case. The presence of the pairing term helps the ground state become separated well enough from the first excited state in the case of even-even nuclei; thus, performing the calculations at $\beta = 2$ MeV^{-1} is sufficient to ensure cooling within a few hundered keV of the ground state. The pairing interaction is given by

$$\hat{V} = -g\hat{P}^{(0,1)\dagger} \cdot \tilde{\hat{P}}^{(0,1)}, \tag{4.3}$$

where $g = 0.212$ MeV was used. $\hat{P}^{(0,1)\dagger}$ above is defined as

$$\hat{P}^{(0,1)\dagger} = \sum_{a} [a^{\dagger}_{j_a} \otimes a^{\dagger}_{j_a}]^{J=0,T=1}. \tag{4.4}$$

Both sets of calculations mentioned above involved 2500-3000 uncorrelated samples and a time discretization of $N_t = 128$ intervals. A comparison of our results with the exact diagonalization values for the quadrupole plus pairing case are illustrated in Table 4.2. The results show that, with sufficient cooling, the SMMCpn results agree with the direct diagonalization values within a few hundred keV.

Calculations using realistic interactions evidently need extrapolations, as explained in Sec. 3.5.1. Hence, another set of comparisons is necessary for demonstrating the viability of the new approach when the extrapolation technique is used. For this purpose, we have calculated ground-state energies, $B(E2)$, $B(M1)$, and $B(GT+)$ strengths of several fp-shell nuclei using the KB3 effective interaction. We compare our results to those obtained by exact diagonalization given in Caurier *et. al.* [12] and those obtained by the isospin SMMC given in Langanke *et. al.* [40]. SMMCpn

Table 4.2: Comparison of the ground-state energies (in MeV), as calculated by SMMCpn and the ANTOINE results. A quadrupole plus pairing interaction is used.

Nucleus	E (ANTOINE)	E (SMMCpn)
^{24}Mg	-39.28	-38.68 ± 0.27
^{26}Mg	-43.58	-42.75 ± 0.70
^{22}Ne	-30.23	-29.53 ± 0.41
^{28}Si	-49.25	-48.80 ± 0.37

calculations were performed at $\beta = 2$ MeV^{-1} with $N_t = 128$ time steps and each calculation at each of six values of g (as explained in Sec. 3.5.1) involved 8000-9000 uncorrelated samples.

In Table 4.3, ground-state energies and $B(E2)$ strengths are tabulated. In all cases, the energies agree strikingly well within error bars that are reasonable with the internal excitation energy of a few hundred keV due to the finite-temperature calculations. $B(E2)$ strength is given by

$$B(E2) = \langle (e_p \hat{Q}_p + e_n \hat{Q}_n)^2 \rangle, \tag{4.5}$$

where the quadrupole operator is defined as $\hat{Q}_{p(n)} = \sum_i r_i^2 Y_2(\theta_i, \phi_i)$. The effective charges were chosen to be $e_p = 1.35$ and $e_n = 0.35$, and the oscillator strength is given by $b = 1.01A^{1/6}$. $B(E2)$ values are also nicely reproduced in general, but in the case of ^{48}Cr, the exact result is underestimated by $\approx 25\%$.

Table 4.4 shows a comparison of results for the $B(M1)$ and $B(GT+)$ strengths. $B(M1)$ strength is defined by

$$B(M1) = \langle (\sum_i \mu_N \{ g_l \vec{l} + g_s \vec{s} \})^2 \rangle, \tag{4.6}$$

where μ_N is the nuclear magneton. We used the bare g factors for angular momentum and spin ($g_l = 1$ and $g_s = 5.586$ for protons and $g_l = 0$ and $g_s = -3.826$ for neutrons). Also defined is the Gamow-Teller strength given by

$$B(GT+) = \langle G_\mp G_\pm \rangle, \tag{4.7}$$

where the unquenched Gamow-Teller operator is written as $G_\pm = \sum_i \vec{\sigma} t_\pm$. Both $B(M1)$ and $B(GT+)$ results agree well with those obtained by direct diagonalization.

Table 4.3: Comparison of exact diagonalization, SMMCpn, and isospin SMMC results for ground-state energies (in MeV) and $B(E2)$ strengths (in e^2fm^4). Typical error bar for energies is ± 0.6 MeV for SMMCpn and ± 0.4 MeV for isospin SMMC calculations.

Nucleus	E exact	E SMMC(pn)	E SMMC (iso)	$\sum$B(E2) exact	$\sum$B(E2) SMMC(pn)	$\sum$ B(E2) SMMC (iso)
^{48}Ti	-24.6	-24.4	-23.9	476	459 ± 33	455 ± 25
^{48}Cr	-32.9	-32.6	-32.3	978	745 ± 40	945 ± 45
^{56}Fe	-66.4	-66.0	-65.8	1019	913 ± 55	990 ± 6
^{64}Zn	-106.3	-106.5	-104.8	1157	1116 ± 81	1225 ± 65

Table 4.4: Comparison of exact diagonalization, SMMCpn, and isospin SMMC results for $B(M1)$ (in μ_N) and Gamow-Teller strengths.

Nucleus	$\sum$B(M1) exact	$\sum$B(M1) SMMC(pn)	$\sum$B(M1) SMMC (iso)	$\sum$B(GT+) exact	$\sum$B(GT+) SMMC(pn)	$\sum$B(GT+) SMMC (iso)
^{48}Ti	10.6	10.4 ± 4	10.2 ± 1.2	1.26	0.89 ± 0.36	1.13 ± 0.18
^{48}Cr	12.0	12.5 ± 4.4	13.8 ± 1.7	4.13	4.35 ± 0.44	4.37 ± 0.35
^{56}Fe	19.4	22.6 ± 6.4	20.4 ± 3.0	4.69	4.02 ± 0.55	3.99 ± 0.27
^{64}Zn	21.6	22.8 ± 1.2	23.6 ± 2.2	5.54	5.66 ± 0.7	4.13 ± 0.34

Lastly, as in the case of isospin SMMC calculations, our calculations satisfy the Ikeda sum rule $B(GT-) - B(GT+) = 3(N - Z)$.

4.2 Applications on Zr and Mo Isotope Chains

As a first novel application of the new implementation, we performed shell-model calculations for the even-even $^{90-104}$Zr and $^{92-106}$Mo isotope chains. The nuclei in this mass region have attracted a lot of attention from the point of view of the interacting shell-model and mean-field studies [27,61] since dramatic changes in the structure of neighboring nuclei have challenged theoretical models to reproduce the experimental data. It is well known that the low-energy structure of these isotopes displays an unusually abrupt shape transition around $N = 60$. ^{90}Zr and ^{92}Mo are spherical at the neutron shell-closure for $N = 50$, and along the Zr isotope chain evidence for sub-shell closure for ^{96}Zr and ^{98}Zr has been reported by various studies. This is followed by a sharp shape transition to the strongly deformed ^{102}Zr. Likewise, along the Mo chain, shapes vary from spherical at ^{92}Mo to rotational-like ^{104}Mo and are known to be deformed up to ^{108}Mo. Evidence of shape coexistence has also been reported [26].

The history of shell-model applications in this mass region goes back to the 60's with model spaces built on ^{88}Sr or ^{90}Zr cores [5, 16, 62, 63]. Gloeckner [28] used an effective interaction built on a ^{88}Sr core with a model space consisting of the orbitals $(\pi : 1p_{1/2}, 0g_{9/2})$, $(\nu : 1d_{5/2}, 2s_{1/2})$. Other studies used larger model spaces [29,35,67] with varying effective interactions and truncation schemes. Holt *et. al.* [32] derived a realistic effective interaction in the model space $(\pi : 1p_{1/2}, 0g_{9/2})$, $(\nu : 1d_{5/2}, 2s_{1/2}, 1d_{3/2}, 0g_{7/2}, 0h_{11/2})$ based on meson exchange models for the free nucleon-nucleon interaction, and carried out calculations for the low-lying spectra of the Zr isotopes with neutron numbers from $N = 52$ to $N = 60$.

In our calculations we have used the same valence space of Holt *et. al.* [32] which is built on the ^{88}Sr core, but employed a slightly modified interaction. Physical parameters that were used in the calculations are given in Table 4.5 ([32] and references therein). All calculations were performed at $\beta = 2$ MeV^{-1} using $N_t = 128$ time intervals and 8500-9500 uncorrelated samples, and the g-extrapolation method was used to obtain the expectation values of the observables.

4.2.1 Ground-state energies

Shown in Fig. 4.1 is the comparison of the expectation value of energy $\langle \hat{H} \rangle$. Filled circles that are connected with dashed lines represent exact diagonalization results obtained by A. Juodagalvis [34] and in both the Zr and Mo cases, the agreement of

Table 4.5: Physical parameters used in the calculations

Protons		Neutrons	
Orbital	Energy (MeV)	Orbital	Energy (MeV)
$0g_{9/2}$	0.90	$0h_{11/2}$	3.50
$1p_{1/2}$	0.00	$0g_{7/2}$	2.63
		$1d_{3/2}$	2.23
		$2s_{1/2}$	1.26
		$1d_{5/2}$	0.00
	$e_p = 1.8$		$e_n = 1.5$
	$b = 2.25$ fm		

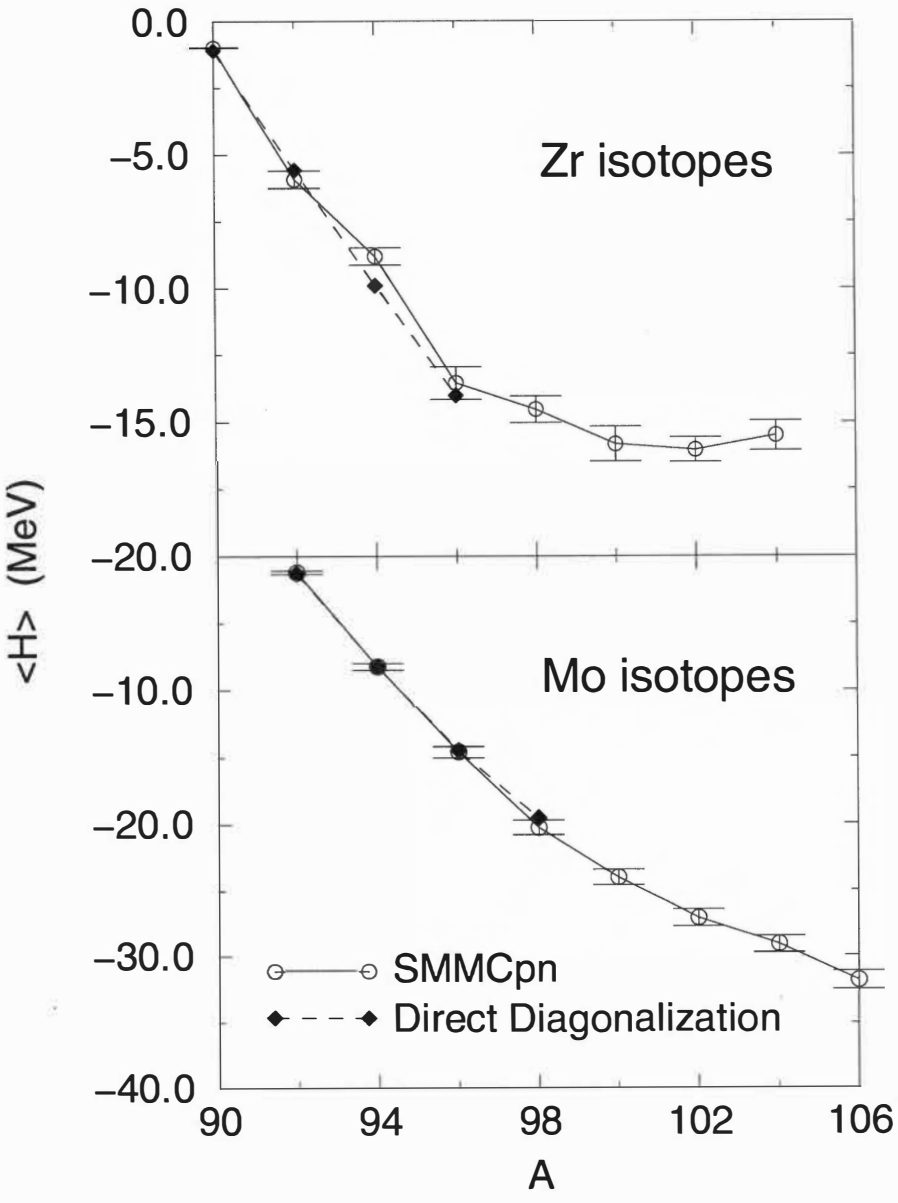


Figure 4.1: Ground-state energies of the even-even $^{90-104}$Zr and $^{92-106}$Mo isotopes. Results from direct diagonalization available for lighter isotopes are also shown.

the SMMCpn values is remarkable. Only for ^{94}Zr, error bars of the SMMCpn result miss the exact value slightly.

4.2.2 Binding energies

The ground-state energies given above correspond to the contribution to the nuclear binding energy of the interaction of the valence particles among themselves.

In Fig. 4.2, we have plotted calculated and experimental values of binding energies with respect to the ^{88}Sr core. We have used the following formulae:

$$\begin{aligned} \mathrm{BE}(^{90+n}\mathrm{Zr}) &= \mathrm{BE}(^{90+n}\mathrm{Zr}) - \mathrm{BE}(^{88}\mathrm{Sr}) \\ &\quad -n\left[\mathrm{BE}(^{89}\mathrm{Sr}) - \mathrm{BE}(^{88}\mathrm{Sr})\right] \\ &\quad -2\left[\mathrm{BE}(^{89}\mathrm{Y}) - \mathrm{BE}(^{88}\mathrm{Sr})\right], \end{aligned} \tag{4.8}$$

$$\begin{aligned} \mathrm{BE}(^{92+n}\mathrm{Mo}) &= \mathrm{BE}(^{92+n}\mathrm{Mo}) - \mathrm{BE}(^{88}\mathrm{Sr}) \\ &\quad -n\left[\mathrm{BE}(^{89}\mathrm{Sr}) - \mathrm{BE}(^{88}\mathrm{Sr})\right] \\ &\quad -4\left[\mathrm{BE}(^{89}\mathrm{Y}) - \mathrm{BE}(^{88}\mathrm{Sr})\right]. \end{aligned} \tag{4.9}$$

An inspection of the resulting relative binding energies shows that the calculated values (shown by asterisks) deviate from the experimental values (shown by filled circles) which display a parabolic behavior. This situation is common among calculations using realistic interactions derived from NN data which is known to be prone to give bad saturation properties. It is known that a given Hamiltonian can always be separated in the form $\hat{H} = \hat{H}_m + \hat{H}_M$ where $\hat{H}_m$ is the monopole part, while the multipole $\hat{H}_M$ contains all other terms [1]. Although $\hat{H}_M$ given by realistic NN interactions takes proper account of the configuration mixing, it is the monopole part $\hat{H}_m$ which should produce the correct unperturbed energies, that fails. It is possible to change the averages of the so-called centroid matrix elements to fix this failure without affecting the spectrosopy in order to produce the correct binding energies [22]. However, a rigorous treatment of the global monopole corrections would require a detailed study and thus go beyond the scope of the current work. Instead, to give some substance to how this correction may work, we add an overall constant to the diagonal interaction elements so that the modified matrix elements are given by

$$V_J^{\mathrm{mod}}(ab, ab) = V_J(ab, ab) + W\frac{n(n-1)}{2}, \tag{4.10}$$

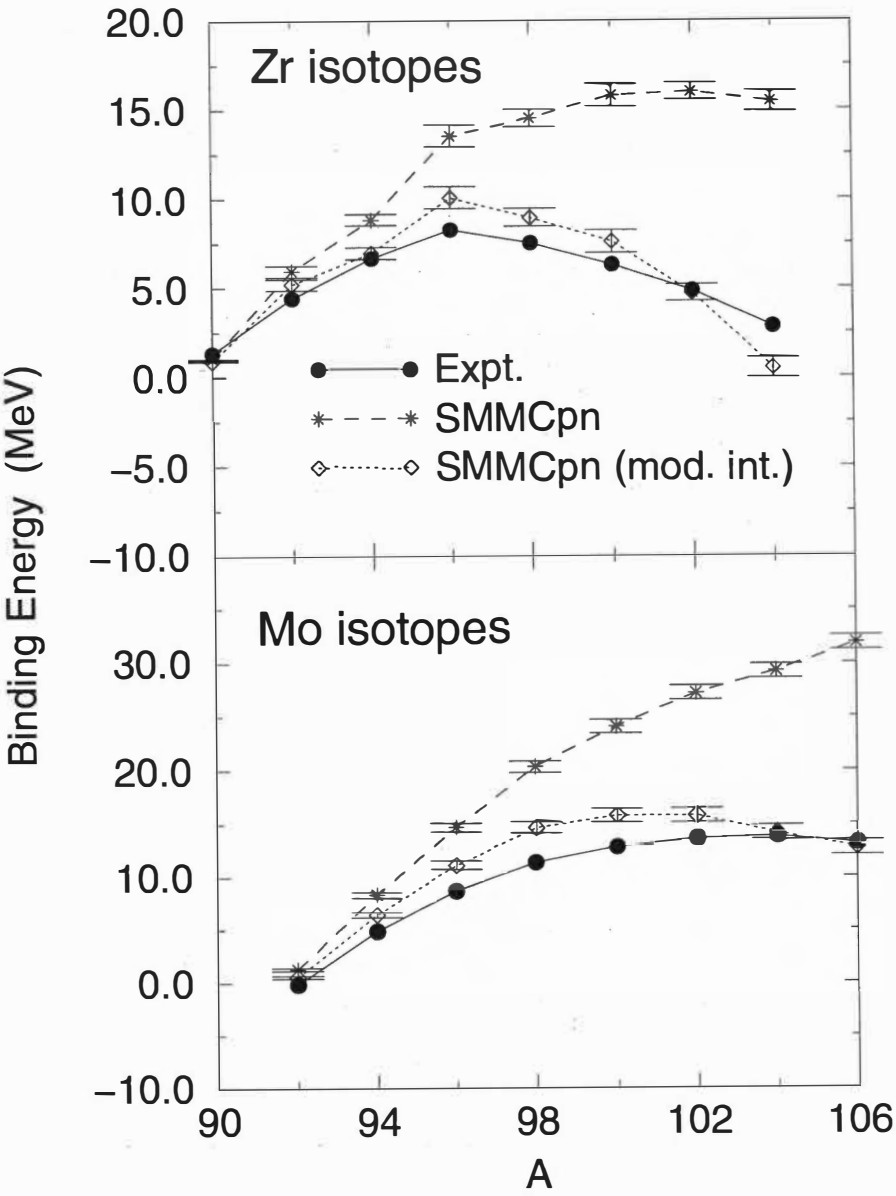


Figure 4.2: Binding energies of the even-even $^{90-104}$Zr and $^{92-106}$Mo isotopes

where n is the number of valence particles. We have adopted $W = -125$ keV to reproduce the binding energy of ^{102}Zr. The effect of this rather naive correction is also plotted in Fig. 4.2, where modified results represented by diamonds show much better agreement for both chains of isotopes.

4.2.3 $B(E2)$ strengths

Since the 2_1^+ state is expected to absorb most of the total $B(E2)$ strength, the latter can be used as a measure of the $0_1^+ - 2_1^+$ spacing, which should reflect a strong change with the shape transitions. Shown in Fig. 4.3 are the calculated total $B(E2)$ strengths (open circles) and available experimental [58] $0_1^+ \rightarrow 2_1^+$ values (filled circles). Despite the fact that the calculated total strengths increase as expected in both isotope chains with the addition of neutrons, their numerical values fall much shorter than the experimental $B(E2; 0_1^+ \rightarrow 2_1^+)$ values on the heavier side of the isotope chains. This failure is probably due to strong components that are missing in the given model space.

4.2.4 Pairing properties

Pairing correlations among like nucleons is known to be important for the ground state properties of the even-even nuclei [19]. These correlations are expected to be quenched along the Zr and Mo isotope chains as the transition from spherical to well-deformed shapes becomes more pronounced. We have investigated the pairing content of the ground states of the nuclei of interest using a BCS-like pair operator which is defined for neutrons as

$$\hat{\Delta}_\nu^\dagger = \sum_{jm>0} \nu_{jm}^\dagger \nu_{j\bar{m}}^\dagger, \tag{4.11}$$

where the sum is over all orbitals with $m > 0$, and $\nu_{j\bar{m}}^\dagger = (-1)^{j+m}\nu_{j-m}^\dagger$ is the time-reversed operator. Hence the expectation value of the pairing fields is $\langle \hat{\Delta}_\nu^\dagger \hat{\Delta}_\nu \rangle$. This quantity for an uncorrelated Fermi gas is given by

$$\langle \hat{\Delta}^\dagger \hat{\Delta} \rangle = \sum_j \frac{n_j^2}{2(2j+1)}, \tag{4.12}$$

where $n_j = \langle \nu_{jm}^\dagger \nu_{jm} \rangle$ are the neutron occupation numbers. Any excess over the Fermi-gas value therefore points out to pairing correlations in the ground state. Our results, which are plotted in Fig. 4.4, confirm a suppression of these correlations, as the contribution of the added neutrons to the pairing gradually decreases and the correlations become noticeably quenched beyond ^{96}Zr and ^{100}Mo.

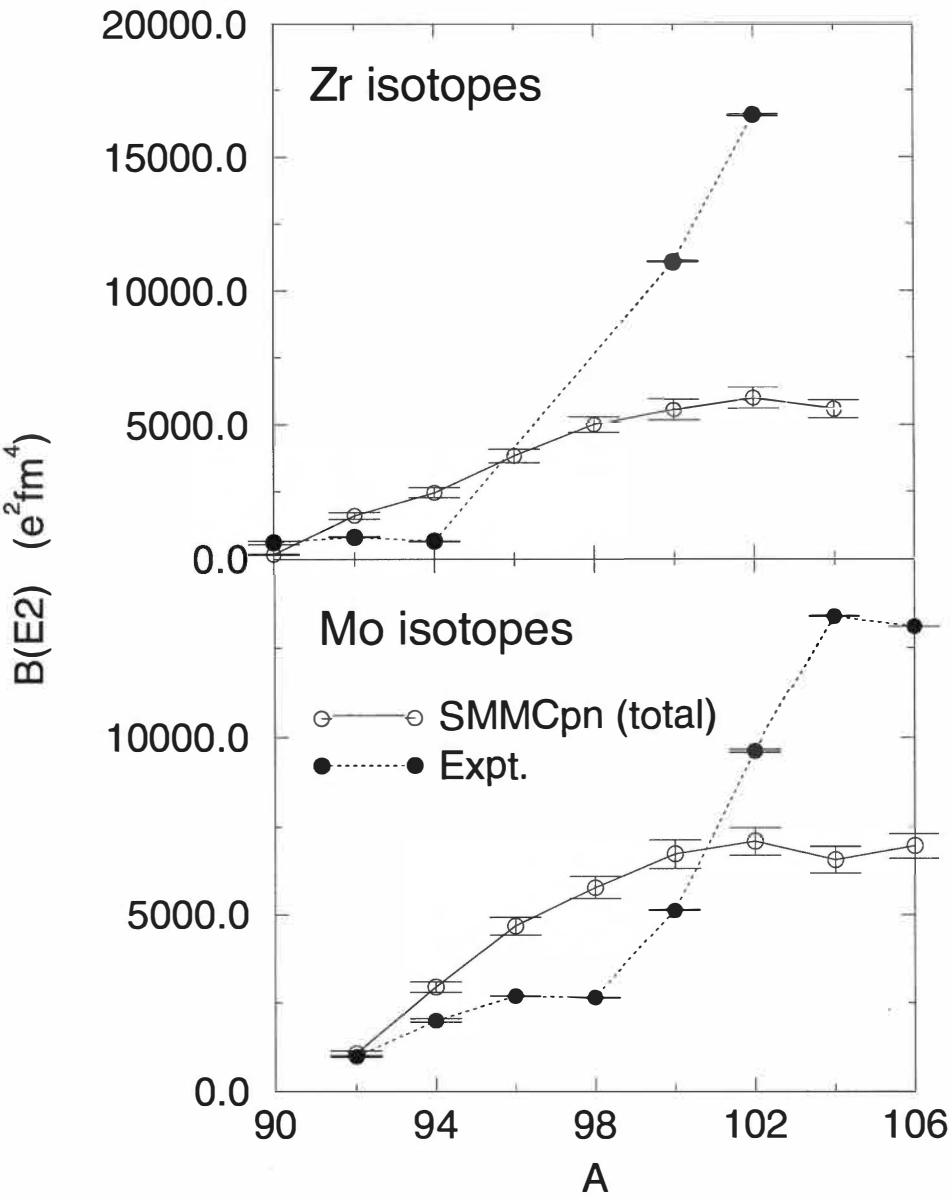


Figure 4.3: Total $B(E2)$ strengths (from the ground state) of the even-even $^{90-104}$Zr and $^{92-106}$Mo isotopes. Experimental results are for $0_1^+ \rightarrow 2_1^+$

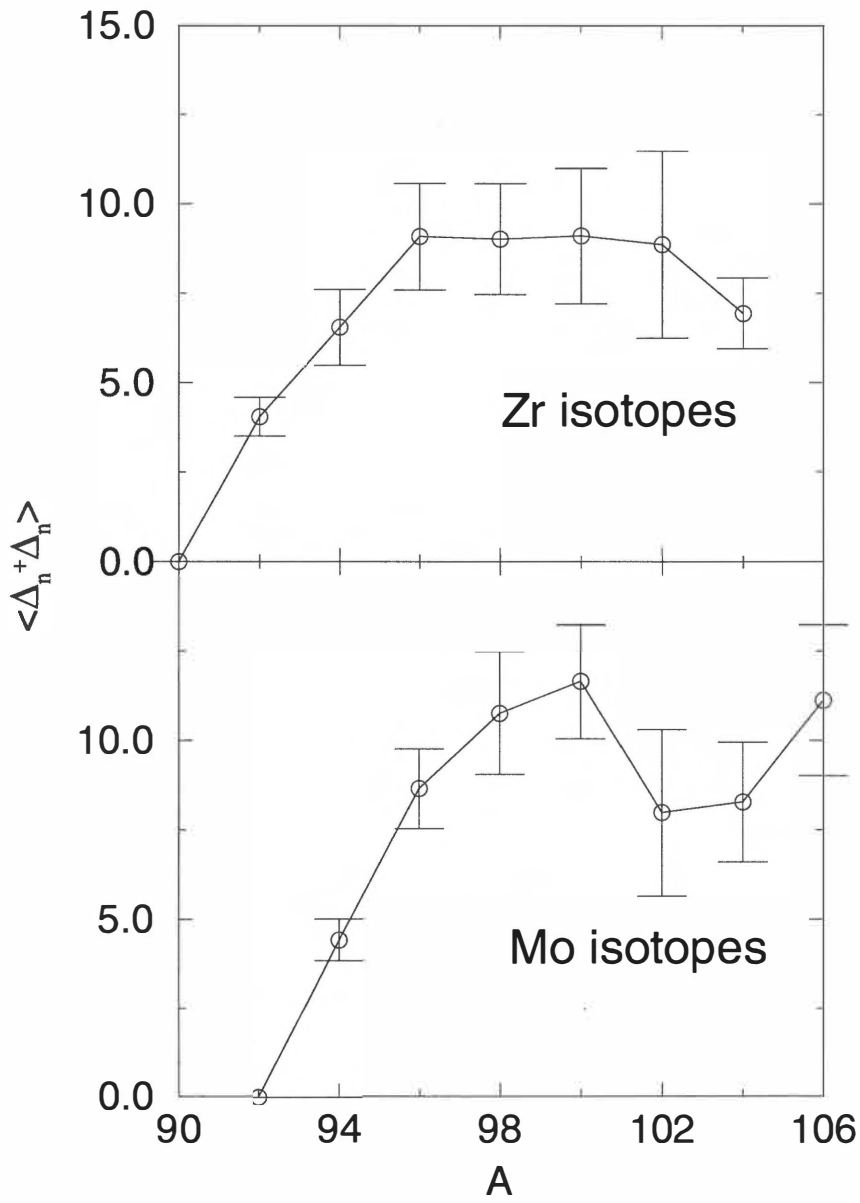


Figure 4.4: Pairing correlations of the even-even $^{90-104}$Zr and $^{92-106}$Mo isotopes. Fermi-gas values are subtracted.

We have also calculated the proton pairing contents of the nuclei in both isotope chains and obtained an essentially constant behavior (within statistical error bars) at a small value, indicating that proton-neutron correlations are not prominent.

In addition, the occupation numbers of various orbitals are plotted in Fig. 4.5, demonstrating that additional neutrons are distributed into the available orbitals rather uniformly, while protons tend to migrate from the $0g_{9/2}$ to the $1p_{1/2}$ orbital. In the case of Mo isotopes, the spurious effect of exceeding the maximum-allowed occupancy for the $1p_{1/2}$ orbital is a result of the extrapolation scheme that was used.

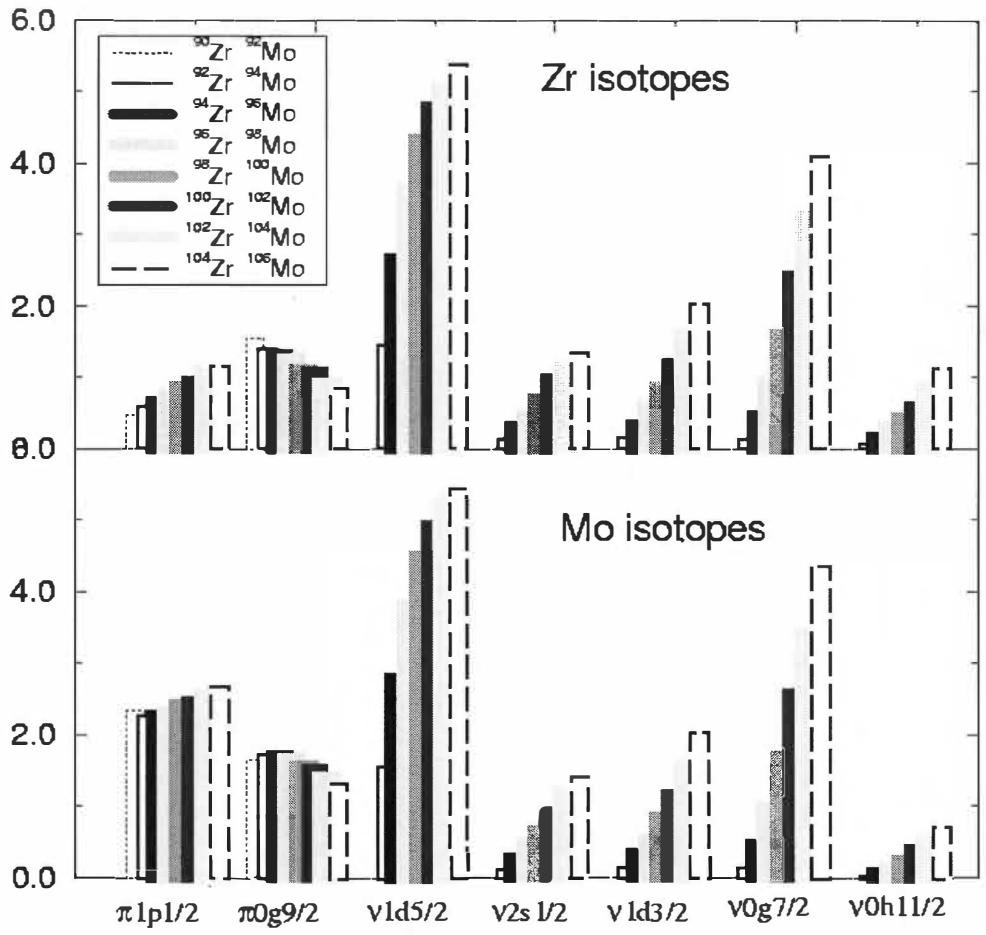


Figure 4.5: Orbital occupation numbers of the even-even $^{90-104}$Zr and $^{92-106}$Mo isotopes

Chapter 5

Summary and Conclusions

We have introduced a new approach for the implementation of the Shell Model Monte Carlo (SMMC) method to perform shell-model calculations using non-identical proton and neutron valence spaces. General features of the SMMC method have been reviewed. Differences between the isospin and the *pn*-formalisms have been pointed out; in particular, the T_z projection has been described in detail.

The results of the SMMCpn approach have been validated in two ways. First, ground-state energies of a few *sd*-shell nuclei were calculated using schematic interactions which satisfies the "good" sign rule. Agreement of the SMMCpn and the ANTOINE results were consistent up to small excitation energies of a few hundred keV. The second set of calculations were performed for a few fp-shell nuclei using the realistic KB3 interaction. The sign problem was dealt with using an extrapolation method. Results for the ground state energies, $B(E2)$, $B(M1)$, and $B(GT+)$ strengths were compared to those obtained by exact diagonalization. In most calculations, the SMMCpn results contained the exact diagonalization results within the statistical error bars.

As the first novel application of the new approach, we have performed a set of calculations for the even-even $^{90-104}$Zr and $^{92-106}$Mo isotopes, using a realistic effective interaction in the valence space described by $(\pi : 1p_{1/2}, 0g_{9/2})$ and $(\nu : 1d_{5/2}, 2s_{1/2}, 1d_{3/2}, 0g_{7/2}, 0h_{11/2})$ orbitals. A comparison of the ground-state energies of the first few nuclei in both isotope chains showed agreement up to thermal excitation energies of a few hundred keV with the exact diagonalization results that were available. We then studied the transitional nature of the isotopes by using the $B(E2)$ strength as a gross measure of the $0_1^+ - 2_1^+$ separation. Along both isotope chains, we have obtained an enhancement in the $B(E2)$ strengths as a function of the added neutrons, accompanied by a quenching in the neutron-pairing correlations. In spite of this qualitative reproduction of the onset of deformations, we have failed in producing reasonable strength in the $E2$ transition rates for the heavier Zr and Mo

nuclei. A comparison with the experimental data suggests that this situation may be a shortcoming due to the degrees of freedom that are absent in the chosen valence space. Yet, another possibility is inspired by mean-field studies [61]; it is well known that the position of the $\nu 0h_{11/2}$ orbital plays a crucial role in the deformations in this mass region; so, the idea of modifying the corresponding single-particle energy is an interesting prospect for future studies.

In summary, we have gained some insight about the model space and the effective interaction, as well as about the feasibility of future shell-model calculations in this mass region.

Apart from future applications involving realistic effective interactions, use of schematic interactions in SMMCpn applications should be an interesting direction of research. Such interactions have been commonly used to calculate realistic estimates of collective properties and level densities; the latter is an important ingredient in the prediction of nuclear reaction rates in astrophysics. Parity dependence of these densities may play a crucial role in the nucleosynthesis. We believe that SMMCpn may prove to be a useful computational tool in this regard.

Bibliography

Bibliography

[1] A. Abzouzi, E. Caurier, and A. P. Zuker, Phys. Rev. Lett. **66** (1991) 1134.

[2] Y. Alhassid, D. J. Dean, S. E. Koonin, G. H. Lang, and W. E. Ormand, Phys. Rev. Lett. **72** (1994) 613.

[3] Y. Alhassid, G. F. Bertsch, S. Liu, and H. Nakada, Phys. Rev. Lett. **84** (2000) 4313.

[4] A. Arima, Nucl. Phys. **A704** (2002) 1c.

[5] N. Auerbach and I. Talmi, Nucl. Phys. **64** (1965) 458.

[6] O. Axel, J. H. D. Jensen, and H. E. Suess, Phys. Rev. **75** (1949) 1776.

[7] A. Bohr and B. R. Mottelson, *Nuclear Structure* (Benjamin, New York, 1969), Vol. 1, p.238.

[8] B. A. Brown, Nucl. Phys. **A704** (2002) 11c.

[9] B. A. Brown, J. Phys. G:Nucl. Part. Phys. **25** (1999) 623.

[10] P. J. Brussaard and P. W. M. Glaudemans, *Shell-Model Applications in Nuclear Spectroscopy*, (North-Holland Publishing, Amsterdam, 1977).

[11] E. Caurier, G. Martinez-Pinedo, F. Nowacki, A. Poves, and A. P. Zuker, nucl-th/0402046 v1

[12] E. Caurier, G. Martinez-Pinedo, F. Nowacki, A. Poves, J. Retamosa, and A. P. Zuker, Phys. Rev. **C59** (1999) 2033.

[13] E. Caurier, computer code ANTOINE, CRN, Strasbourg (1989).

[14] J.-Q. Chen, A. Novoselsky, M. Vallieres, and R. Gilmore, Phys. Rev. **C38** (1998) 1440.
M. Vallieres, A. Novoselsky, and R. Gilmore, *Proceedings of the International*

Conference on Computers in Physics, ed. L. Deyuan and D. H. Feng (World Scientific, Singapore, 1989)

[15] F. Coester, Nucl. Phys. **7** (1958) 421; J. Čízek, J. Chem. Phys. **45** (1966) 4256.

[16] S. Cohen, R. D. Lawson, M. H. Macfarlane and M. Soda, Phys. Lett. **10** (1964) 195.

[17] E. V. Condon and G. H. Shortley, *The Theory of Atomic Spectra*, Ch. III (Cambridge University Press, 1935).

[18] D. J. Dean, M. T. Ressell, M. Hjorth-Jensen, S. E. Koonin, K. Langanke, and A. P. Zuker, Phys. Rev. **C59** (1999) 2474.

[19] D. J. Dean and M. Hjorth-Jensen, Rev. Mod. Phys. **75** (2003) 607.

[20] D. J. Dean and M. J. Hjorth-Jensen, nucl-th/0308088 v1.

[21] D. J. Dean, T. Engeland, M. Hjorth-Jensen, M. P. Kartamyshev, and E. Osnes, Prog. in Part. and Nucl. Phys. **53** (2004) 419.

[22] J. Duflo and A. P. Zuker, Phys. Rev. **C59** (1999) R2347.

[23] J. Dukelsky, S. Pittel, S. S. Dimitrova, and M. V. Stoitsov, Phys.Rev. **C65** (2002) 054319.

[24] C. Forssen, P. Navratíl, W. E. Ormand, and E. Caurier, Phys. Rev. **C71** (2005) 044312.

[25] J. B. French, E. C. Halbert, J. B. McGrory, and S. S. M. Wong, Adv. Nucl. Phys. **3** (1969) 237.

[26] J. B. Gupta, J. Phys. G: Nucl. Part. Phys. **28** (2002) 2365, and references therein.

[27] L. S. Geng, H. Toki, and J. Meng, Mod. Phys. Lett. **A19** (2004) 2171.

[28] D. H. Gloeckner, Nucl. Phys. **A253** (1975) 301.

[29] P. Halse, J. Phys. G **19** (1993) 1859.

[30] K. Heyde, *The Nuclear Shell Model*, (Springer, Berlin, 1991).

[31] M. Hjorth-Jensen, T. T. S. Kuo, and E. Osnes, Phys. Rep. **261** (1995) 125.

[32] A. Holt, T. Engeland, M. Hjorth-Jensen, and E. Osnes, Phys. Rev. **C61** (2000) 064318.

[33] J. Hubbard, Phys. Lett. **3** (1959) 77; R. D. Stratonovich, Dokl. Akad. Nauk., SSSR **115** (1957) 1907 [transl: Soviet Phys. Kokl. **2** (1958) 416].

[34] A. Juodagalvis, private communication.

[35] S. S. Ipson, K. C. McLean, W. Booth, J. G. B. Haigh, and R. N. Glover, Nucl. Phys. **A253** (1975) 301.

[36] G. Sugiyama and S. E. Koonin, Ann. Phys. **168** (1986) 1.

[37] S. E. Koonin, D. J. Dean, and K. Langanke, Phys. Rep. **278** (1997) 2

[38] K. Kowalski, D. J. Dean, M. Hjorth-Jensen, T. Papenbrock, and P. Piecuch, Phys. Rev. Lett **92** (2004) 132501.

[39] G. H. Lang, C. W. Johnson, S. E. Koonin, and W. E. Ormand, Phys. Rev. **C48** (1993) 1518.

[40] K. Langanke, D. J. Dean, P. B. Radha, Y. Alhassid, and S. E. Koonin, Phys. Rev. **C52** (1995) 718.

[41] R. D. Lawson, *Theory of the Nuclear Shell Model*, (Clarendon Press, Oxford, 1980).

[42] E. Y. Loh, Jr. and J. E. Gubernatis, in *Electronic Phase Transitions*, edited by W. Hanke and Y. V. Kopaev (North Holland, Amsterdam, 1992).

[43] M. Mayer, Phys. Rev. **75** (1949) 1969.

[44] N. Metropolis, A. Rosenbluth, M. Rosenbluth, A. Teller, and E. Teller, J. Chem. Phys. **21** (1953) 1087.

[45] H. Nakada and Y. Alhassid, Phys. Rev. Lett. **79** (1997) 2939.

[46] P. Navratíl, J. P. Vary, and B. R. Barrett, Phys. Rev. **C62** (2000) 054311.

[47] J. W. Negele and H. Orland, *Quantum Many-Particle Systems*, (Addison-Wesley, Redwood City, 1988).

[48] F. Nowacki and E. Caurier, coupled code NATHAN, Strasbourg (1995).

[49] W. E. Ormand, Progress of Theoretical Physics Supplement **124** (1996) 37.

[50] W. E. Ormand, D. J. Dean, C. W. Johnson, G. H. Lang, and S. E. Koonin, Phys. Rev. **C49** (1994), 1422.

[51] M. Honma, T. Mizusaki, and T. Otsuka, Phys. Rev. Lett. **75** (1995) 1284.

[52] T. Otsuka, T. Mizusaki, and M. Honma, Phys. Rev. Lett. **81** (1998) 1588.

[53] T. Otsuka, R. Fujimoto, Y. Utsuno, B. A. Brown, M. Honma, and T. Mizusaki, Phys. Rev.Lett. **87** (2001) 082502.

[54] T. Papenbrock and D. J. Dean, nucl-th/0412112 v1.

[55] S. C. Pieper and R. B. Wiringa, Ann. Rev. Nucl. Part. Sci. **51** (2001) 53.

[56] S. C. Pieper, Nucl. Phys. **A751** (2005) 516.

[57] W. D. M. Rae, A. Etchegoyen, and B. A. Brown, OXBASH, The Oxford-Buenos Aires-MSU shell-model code, Michigan State University Cyclotron Laboratory Report No. 524 (1988).

[58] S. Raman, C. W. Nestor, Jr. and P Tikkanen, At. Data Nucl. Data Tables **78** (2001) 1.

[59] N. Rom, D. M. Charutz, and D. Neuhauser, Chem. Phys. Lett. **270** (1997) 382.

[60] A. de-Shalit and I. Talmi, *Nuclear Shell Theory*, (Academic Press, New York, 1963).

[61] J. Skalski, S. Mizutori, and W. Nazarewicz, Nucl. Phys. **A617** (1997) 282.

[62] I. Talmi and I. Unna, Nucl. Phys. **19** (1960) 225.

[63] J. Vervier, Nucl. Phys. **75** (1966) 17.

[64] J. D. Walecka, *Theoretical Nuclear and Subnuclear Physics*, (Oxford University Press, New York, 1995).

[65] R. R. Whitehead, A. Watt, B. J. Cole, and I. Morrison, Adv. Nucl. Phys. **9** (1977) 123.

[66] M. Wloch, D. J. Dean, J. R. Gour, M. Hjorth-Jensen, K. Kowalski, T. Papenbrock, and P. Piecuch, Phys. Rev. Lett **94** (2005) 212501.

[67] Chang-hua Zhang, Shun-jin Wang, and Jin-nan Gu, Phys. Rev. **C60** (1999) 054316.

Vita

Cem Özen was born in Ankara, Turkey, on September 12, 1972, the son of Mehmet Özen and Gökçen Özen. He received his education at the Middle East Technical University in Ankara, obtaining his Bc.S. and M.S. degrees in Physics. He started his doctoral studies at the George Washington University as a Bell-Atlantic Fellow. In the summer of 1998, he joined the University of Tennessee as a Science Alliance Fellow where he held graduate teaching and research assistanships subsequently. He received his Ph.D. in Physics at the University of Tennessee in August 2005. In the fall of 2005, he will join GSI at Darmstadt as a Postdoctoral Fellow. He enjoys cycling, archaeology, and history.

4535 0545 30
11/09/05 MAB